JOURNAL OF GEOPHYSICAL RESEARCH, VOL. 103, NO. D11, PAGES 13,285–13,313, JUNE 20, 1998

UARS Microwave Limb Sounder HNO_3 observations: Implications for Antarctic polar stratospheric clouds

M. L. Santee,[1] A. Tabazadeh,[2] G. L. Manney,[1] R. J. Salawitch,[1] L. Froidevaux,[1] W. G. Read,[1] and J. W. Waters[1]

Abstract. We present Microwave Limb Sounder (MLS) measurements of gas-phase HNO_3 obtained at the beginning of five southern hemisphere winters: 1992–1996. To investigate the composition of the polar stratospheric clouds (PSCs) that formed in early winter each year, the observed evolution of HNO_3 at 465 K is compared against that predicted using nitric acid trihydrate (NAT), nitric acid dihydrate (NAD), and liquid ternary solution models of PSC formation and correlated with temperature histories from three-dimensional back trajectory calculations. The MLS HNO_3 observations suggest that the initial composition of PSCs depends on the physical state of the background sulfate aerosols. If the preexisting aerosols are liquid, then the formation of ternary solutions is initiated as the temperature drops below about 192 K, followed by a gradual conversion to NAD after exposure to low temperatures for several days. HNO_3 uptake into ternary solutions occurs at higher temperatures, and the conversion to NAD is delayed, under conditions of enhanced aerosol loading from the Mount Pinatubo eruption. If a majority of the background aerosols are frozen, the growth of ternary solutions is inhibited, but formation of a metastable, water-rich, HNO_3-containing solid phase characterized by a relatively high HNO_3 vapor pressure (type Ic PSC) may occur. In general, MLS HNO_3 measurements obtained during early southern winter indicate a strong correspondence between the area of gas-phase HNO_3 loss and the area of temperatures below 192 K but only a weak correspondence between the area of gas-phase HNO_3 loss and the area of temperatures below 195 K, the value commonly assumed as the threshold for PSC formation. Although temperatures were low enough to maintain NAT PSCs, the MLS data show that they were not forming, at least not over spatial scales comparable to or larger than the $\sim 400 \times 100 \times 5$ km MLS field of view.

1. Introduction

It is well established that the chlorine-catalyzed destruction of ozone in the polar lower stratosphere during winter and spring is initiated through heterogeneous chemical reactions on the surfaces of polar stratospheric cloud (PSC) particles [e.g., *Solomon*, 1990]. Accurate theoretical predictions of ozone loss therefore require knowledge of the phase and composition of the PSC particles. For instance, recent work [*Ravishankara and Hanson*, 1996; *Borrmann et al.*, 1997] has shown that liquid particles may activate chlorine more efficiently than frozen particles. However, despite a considerable number of field, laboratory, and modeling studies, the exact PSC formation mechanism remains uncertain.

There are two main classifications of PSCs: type I and type II. Type II PSCs are composed of water ice and typically form a few degrees below the equilibrium condensation point of ice (nominally 188 K for lower stratospheric conditions) because supersaturations with respect to ice exceeding unity are required to overcome the free-energy barrier to nucleation [e.g., *Toon et al.*, 1989]. In contrast, type I PSCs are observed to form at temperatures several degrees above the water ice frost point [e.g., *McCormick et al.*, 1982]. *Toon et al.* [1986] and *Crutzen and Arnold* [1986] suggested that type I PSCs contain HNO_3, and the principal phase was usually assumed to be nitric acid trihydrate (NAT, $HNO_3 \cdot 3H_2O$), which condenses at $\sim$195 K and which is the most stable form under stratospheric conditions [*Hanson and Mauersberger*, 1988]. Early field observations [e.g., *Fahey et al.*, 1989; *Pueschel et al.*, 1989] confirmed that HNO_3 is a major component of type I PSC particles and that the temperature at which they first appear is roughly consistent with formation of a trihydrate phase. For years the canonical model of PSC formation was predicated on a NAT composition for the type I particles [e.g., *Solomon*, 1990].

However, there is a growing body of evidence that not all type I PSC particles are composed of NAT. In the Arctic, large NAT supersaturations have been observed before the onset of significant particle growth [e.g., *Dye et al.*, 1992], and the amount of HNO_3 incorporated into the particles has been found to be significantly less than that predicted for a NAT composition [*Kawa et al.*, 1992]. Two

[1]Jet Propulsion Laboratory, California Institute of Technology, Pasadena.

[2]NASA Ames Research Center, Moffett Field, California.

Paper number 98JD00365.
0148-0227/98/98JD-00365$09.00

subclasses of type I PSCs have been recognized based on lidar measurements of aerosol optical properties [*Browell et al.*, 1990; *Toon et al.*, 1990a]: type Ia, relatively large, nonspherical particles, and type Ib, smaller, nearly spherical particles. Laboratory measurements [*Zhang et al.*, 1993a; *Molina et al.*, 1993] have shown that HNO_3 is highly soluble in aqueous H_2SO_4 at the low temperatures typical of polar winter, and a supercooled ternary ($H_2SO_4/HNO_3/H_2O$) solution composition has been proposed for type Ib particles [*Tabazadeh et al.*, 1994a]. Previously obtained field observations have now been reinterpreted as being more consistent with a ternary than with a NAT composition for both the Arctic [*Drdla et al.*, 1994; *Carslaw et al.*, 1994; *Tabazadeh et al.*, 1994a] and the Antarctic [*Toon and Tolbert*, 1995]. Ground-based lidar [*Beyerle et al.*, 1997] and balloon-borne backscatter [*Larsen et al.*, 1997] measurements have provided further evidence for liquid ternary solution PSCs in the Arctic. In addition, analyses of total reactive nitrogen and aerosol particle volume measured during the 1994 Airborne Southern Hemisphere Ozone Experiment (ASHOE) have indicated that a type I PSC near the edge of the Antarctic vortex was composed primarily of ternary solution droplets [*Dye et al.*, 1996; *Del Negro et al.*, 1997]. Trends in ground-based measurements of stratospheric HNO_3 over the south pole have also suggested the formation of ternary solution PSCs [*de Zafra et al.*, 1997].

Although formation of liquid type Ib PSCs is now thought to be understood, the mechanisms by which crystalline type Ia PSCs form in the stratosphere remain unresolved [*Tolbert*, 1994]. Previously, it was assumed that frozen sulfuric acid aerosols provide nucleation sites for the formation of type Ia PSCs [e.g., *Turco et al.*, 1989; *Toon et al.*, 1989]. However, laboratory experiments on sulfuric acid films [*Middlebrook et al.*, 1993] have indicated that temperatures near the ice frost point are necessary for the stratospheric sulfate aerosol to freeze, forming sulfuric acid tetrahydrate (SAT); recent experiments on binary sulfate aerosol particles [*Imre et al.*, 1997; *Carleton et al.*, 1997; *Clapp et al.*, 1997] have confirmed that stratospheric sulfate aerosols most likely remain liquid to the ice frost point or below. Laboratory observations of ternary bulk solutions [*Koop et al.*, 1995] and freely floating ternary droplets [*Anthony et al.*, 1997] have also found that supercooled ternary solutions do not freeze for temperatures above the ice frost point. Other laboratory studies [*Molina et al.*, 1993; *Beyer et al.*, 1994; *Iraci et al.*, 1995] have shown that NAT crystallization directly from the vapor phase onto SAT is unlikely; these studies suggest that NAT nucleates out of liquid ternary solutions, with subsequent growth of the crystals by condensation of HNO_3 and H_2O vapors. However, model calculations [*Tabazadeh and Toon*, 1996] indicate that the highest possible HNO_3 concentration in a ternary droplet is insufficient to allow the direct crystallization of NAT. Several candidates have been proposed for an initial metastable phase for condensed HNO_3 in PSCs, with eventual conversion to NAT. For example, laboratory results of *Marti and Mauersberger* [1993] suggest a dilute HNO_3/H_2O solid phase (with a water to nitric acid ratio of about 5 or 6 to 1) as a transient PSC composition. Recent laboratory experiments by *Fox et al.* [1995] also suggest that NAT nucleation from a ternary solution requires the formation of a precursor phase, which they infer to be a mixed H_2SO_4/HNO_3 hydrate (MixH, $H_2SO_4 \cdot HNO_3 \cdot 5H_2O$). In cooling a ternary solution under stratospheric conditions, *Fox et al.* [1995] never observed NAT nucleation in the solution without prior formation of MixH, which then transformed into a metastable nitric acid dihydrate (NAD, $HNO_3 \cdot 2H_2O$) phase within a few hours. NAT was always the last phase to form, with NAD persisting for days, in agreement with their earlier laboratory experiments on PSCs [*Worsnop et al.*, 1993] showing NAD to be only slightly less stable than NAT.

Alternatively, laboratory studies by *Koop et al.* [1995] show that ternary bulk solutions remain supercooled to temperatures below the ice frost point. They contend that only water ice is a suitable nucleation site for H_2SO_4 and HNO_3 hydrates, and thus stratospheric aerosol droplets must cool below the frost point before crystallization of either HNO_3 or H_2SO_4 in solution is possible. *Meilinger et al.* [1995] suggest that the rapid cooling rates induced by orographically forced lee waves lead to nonequilibrium conditions that facilitate freezing of the smallest ternary droplets into NAT, since their composition is closest to that of trihydrate. However, recent freezing experiments on HNO_3/H_2O aerosols indicate that the HNO_3 concentration in solution must be larger than 1:2.5 (HNO_3:H_2O) in order for HNO_3 to crystallize [*Disselkamp et al.*, 1996]. This result argues against the *Meilinger et al.* [1995] proposal of crystallization of aerosols containing less than a 1:3 (HNO_3:H_2O) ratio. In addition, *Tabazadeh et al.* [1996] use aircraft observations of PSCs and a statistical analysis in which both background and lee wave temperature fluctuations are superimposed on synoptic-scale temperature histories to demonstrate that neither ice crystal nucleation nor lee wave encounters are correlated with the occurrence of type Ia PSCs. *Murphy and Gary* [1995] and *Tabazadeh et al.* [1996] argue that small but rapid temperature fluctuations (especially frequent in the Arctic) promote the initial formation of large numbers of small metastable particles with subsequent mass transfer to the larger, more stable NAT particles. In fact, *Tabazadeh et al.* [1996] conclude that mass transfer, and not the mesoscale cooling rate, controls the type Ia PSC formation process; once synoptic temperatures drop below about 192 K, the only condition necessary for type Ia formation is that temperatures remain below the NAT frost point for longer than ~1 day. *Larsen et al.* [1997] reach a similar conclusion based on balloon measurements of Arctic PSCs, finding that particle properties are most strongly influenced by the synoptic temperature history even for measurements obtained in regions where lee waves are common.

Building on the laboratory studies [*Worsnop et al.*, 1993; *Marti and Mauersberger*, 1993] indicating the initial presence of higher hydrates of HNO_3, *Tabazadeh et al.* [1995] and *Tabazadeh and Toon* [1996] have postulated a third subclass of type I PSCs, type Ic, composed of a water-rich metastable HNO_3/H_2O solid phase that transforms into NAT or NAD over time. In their scenario, the thermal history

of the air mass, and thus the physical state of the background sulfate aerosols, determines the phase of the PSCs: Upon cooling, if the H_2SO_4 aerosols are liquid, then type Ib ternary solutions form; if they are frozen, then type Ic particles initially form. Assuming that the ice frost point is not reached, if the cooling is then followed by a warming to about 196–198 K, some supercooled H_2SO_4/H_2O aerosols may freeze (as observed in the laboratory by *Iraci et al.* [1994]) and remain frozen until the air mass experiences temperatures high enough to melt SAT (about 210–220 K [*Middlebrook et al.*, 1993; *Zhang et al.*, 1993b]). With this mechanism, cooling/warming cycles eventually lead to the formation of type Ia PSCs. This scenario is consistent with aircraft observations of PSCs in both the Arctic and the Antarctic [*Tabazadeh et al.*, 1995, 1996] and is supported by analyses of balloon-borne backscatter measurements of PSCs from several Arctic winters [*Larsen et al.*, 1996, 1997]. Ground-based Arctic lidar measurements by *Shibata et al.* [1997] have also indicated the presence of large water-rich particles that are not compatible with the standard type Ia/b PSC classifications.

In this study we investigate PSC formation using measurements of gas-phase HNO_3 made by the Microwave Limb Sounder (MLS) aboard the Upper Atmosphere Research Satellite (UARS). Although these satellite measurements lack the resolution and precision of in situ measurements, they have the important advantage of providing daily hemispheric coverage over a range of pressures and over the course of several years. A description of the MLS HNO_3 measurements and their quality and spatial resolution is provided in section 2, and their suitability for studies of PSC composition is discussed in section 3. In section 4 we examine in detail the evolution of gas-phase HNO_3 during the 1994 early southern winter period, and we contrast this behavior with that during similar periods in 1992, 1993, 1995, and 1996. We compare the observed HNO_3 values in each year with those predicted by several proposed PSC composition models. Specifically, we discuss the MLS HNO_3 data in relation to type Ia PSCs based on the work of *Hanson and Mauersberger* [1988] and *Worsnop et al.* [1993], type Ib PSCs based on the work of *Tabazadeh et al.* [1994b], and type Ic PSCs based on the work of *Tabazadeh and Toon* [1996]; no new PSC subclasses are proposed here. Any comparison of MLS data with model results necessarily entails several assumptions; the observational and/or modeling studies underlying our assumptions, and the sensitivity of our results to them, are also discussed in section 4. Finally, in section 5 we use back trajectory calculations to explore the correlation between temperature history and PSC composition as inferred from MLS measurements of gas-phase HNO_3.

We find that the MLS HNO_3 observations indicate variations in PSC composition with time and meteorological conditions. Although our results are strongly suggestive, it must be borne in mind that the coarse spatial resolution and precision of the data, together with the necessity of estimating unmeasured quantities, limit our ability to definitively identify PSC compositions.

2. Measurement Description

2.1. General MLS Information

MLS has been acquiring millimeter-wavelength emission measurements of the stratosphere in both hemispheres since late September 1991. Measurements are made as the instrument field of view (FOV) is vertically scanned through the atmospheric limb in a plane perpendicular to the UARS velocity. The microwave limb sounding technique and the MLS instrument are described in detail by *Waters* [1993] and *Barath et al.* [1993], respectively. Advantages of this technique include the measurement of thermal emission, so that observations can be obtained both day and night, and the use of long wavelengths, so that the data are not degraded by the presence of PSCs or other stratospheric aerosols. Validation of the MLS instrument calibration and the primary MLS measurements is described in a special issue of *Journal of Geophysical Research* (*101* (D6), 9,539–10,476) dedicated to the evaluation of the UARS data.

The MLS pointing geometry together with the inclination of the UARS orbit leads to a measurement latitudinal coverage extending from 80° on one side of the equator to 34° on the other. The UARS orbit plane precesses in such a way that all local solar times are sampled in ~36 days (a "UARS month"), getting ~20 min earlier each day at a given latitude. To keep MLS (and other instruments) on the shaded side of the spacecraft, a 180° yaw maneuver is performed at the end of every UARS month. Thus 10 times per year MLS alternates between viewing northern and southern high latitudes, with the first day of a particular UARS month occurring ~5 days earlier each year.

2.2. MLS HNO_3 Data Quality

Although HNO_3 was not a primary MLS measurement objective, a significant HNO_3 feature situated just outside the spectral region used to measure ozone imposes a weak slope through the 205-GHz ozone band that can be used to retrieve profiles of gas-phase HNO_3. MLS HNO_3 measurements (from precursory algorithms) were first presented by *Santee et al.* [1995]. With the release of MLS version 4 retrieval algorithms, HNO_3 is now a standard product available for every day of the mission on which MLS made measurements. Version 4 MLS HNO_3 data for the 1995–1996 and 1996–1997 northern winters have been presented by *Santee et al.* [1996] and *Santee et al.* [1997], respectively.

Preliminary validation studies indicate that the MLS HNO_3 data are scientifically useful on the 100-, 46-, and 22-hPa retrieval surfaces, where the estimated single-profile precisions are approximately 2.0, 3.0, and 4.5 ppbv, respectively. The precisions, estimated from several months of data, were based on the observed variability in a narrow latitude band centered around the equator that was selected to minimize the effects of natural atmospheric variability. The true precisions may be slightly better than these estimates since the actual atmospheric variation is not completely negligible. These empirical precisions are generally consistent with uncertainties derived theoretically by propagating

the measurement noise through the retrieval algorithm. Although the computed uncertainties consist of both random and systematic components, the random (noise) components usually dominate for HNO_3, which has a relatively weak signal (compared with ozone, for example). The noise contribution to the uncertainty can be reduced by averaging together individual measurements.

These calculated uncertainty values are included in the daily MLS Level 3A HNO_3 data files (the Level 3A files for each geophysical parameter consist of retrieved values on a vertical grid common to all UARS instruments producing atmospheric profiles). The retrieval algorithm, which is based on sequential estimation, employs an a priori estimate from a month- and latitude-dependent climatology developed by the UARS science team. Under conditions of poor measurement sensitivity when the contribution to the retrieved values from the a priori estimate exceeds 25%, the uncertainties are flagged with a negative sign. Quality control is imposed on the MLS HNO_3 data by discarding retrievals having negative uncertainty values. In addition, the Level 3P parameter file associated with each Level 3A file, which contains other diagnostics identifying bad data records, is examined, and only profiles for which the flag `MMAF_STAT` = "G," "T," or "t" and the flag `QUALITY_O3_205` = 4 (since HNO_3 is retrieved in the 205-GHz ozone band) are used. However, these quality control measures are not always sufficient to filter out large spikes in the retrieved HNO_3 mixing ratios; occasional anomalous retrievals are eliminated on an individual basis. More detailed information about the quality of the MLS data is available from the NASA Goddard Space Flight Center Distributed Access Archive Center (DAAC) as well as the MLS web page (http://mls.jpl.nasa.gov).

Initial comparisons (over a limited data set) with colocated UARS Cryogenic Limb Array Etalon Spectrometer (CLAES) HNO_3 observations [*Kumer et al.*, 1996] show that the MLS HNO_3 agrees well at 100 hPa but is usually 0-2 ppbv lower at 46 hPa and 0-4 ppbv higher at 22 hPa (particularly in the polar regions). However, even where biases between the two data sets exist, there is good correspondence in the morphology of the CLAES and MLS HNO_3 fields. Preliminary comparisons with other correlative data sets also indicate that MLS overestimates HNO_3 abundances near the profile peak (around 25 km). Further validation of the MLS HNO_3 data set is in progress.

2.3. Spatial Resolution of MLS HNO_3 Data

For optically thin cases such as the HNO_3 measurement, the relative contribution to the measured limb emission (the weighting function) along the observation path has a Gaussian distribution, the width of which sets the horizontal resolution along the line of sight to ~400 km [*Waters*, 1993]. The UARS orbital motion during the portion of the limb scan in which HNO_3 is measured smears the measurements over ~100 km in a direction perpendicular to the MLS line of sight. The FOV vertical extent at the tangent point is ~3 km, but version 4 data are produced on a vertical grid with points spaced three per decade in the logarithm of atmospheric pressure, yielding a vertical resolution of ~5 km. Thus the retrieved MLS HNO_3 values at a particular geographic location and atmospheric level essentially represent averages over a $\sim 400 \times 100 \times 5$ km volume of air.

3. Using MLS Data to Study PSCs

An assumption inherent in using MLS observations of gas-phase HNO_3 depletion to infer PSC composition is that the instrument FOV is filled by a single PSC type. Therefore the suitability of the MLS data for these kinds of studies depends on the scale of the spatial inhomogeneity in the clouds. The prevalence of PSCs inside the winter polar vortices was first recognized in satellite solar occultation observations of aerosol extinction from the Stratospheric Aerosol Measurement (SAM) II experiment [*McCormick et al.*, 1982]. In particular, these observations show that Antarctic PSCs typically form at 20 km in the late May/early June time period and rapidly develop into extensive regions of enhanced extinction coincident with areas of low temperature [*McCormick et al.*, 1982, 1989; *Poole and Pitts*, 1994]. However, the extent of a typical cloud bank cannot be determined from SAM II data alone since the measurement coverage on a given day is restricted to a fixed latitude that is generally near the edge of the vortex in winter (away from the coldest regions in the vortex interior) and since the instrument field of view is ~200 km [*McCormick et al.*, 1989]. UARS CLAES measurements of aerosol extinction have also revealed widespread PSC activity [*Mergenthaler et al.*, 1993; *Roche et al.*, 1994; *Mergenthaler et al.*, 1997], but, again, these data have limited horizontal resolution (~500 km [*Roche et al.*, 1993]).

The spatial scale of a "typical" type I PSC is probably best estimated from airborne lidar data. Few such data have been reported for the Antarctic; although *Browell et al.* [1988] observed many PSCs of large vertical and horizontal extent (>5 km in altitude and >5°–10° in latitude), these data were collected on flights between late August and late September. Possibly of more relevance to PSC formation in the Antarctic early winter time period are the lidar data from several Arctic aircraft missions. PSCs were observed continuously over the entire latitude range from 76°N to 90°N in multiple layers between 19 km and 23 km during a flight on January 24, 1984 [*McCormick et al.*, 1985; *Kent et al.*, 1986], although temperatures were sufficiently low that these may have been primarily water ice clouds. Two different sets of lidar data were obtained during the Airborne Arctic Stratospheric Expedition (AASE) of the winter of 1988–1989. *McCormick et al.* [1990] report lidar measurements from flights on January 24 and 31, 1989, that indicate type I PSCs spanning about 15° in latitude and 5 km in altitude. These measurements do not distinguish between type Ia and Ib PSCs, but they do reveal localized areas of type II PSCs embedded in the type I cloud. Data from a multiwavelength lidar system have been used [*Browell et al.*, 1990; *Toon et al.*, 1990a] to identify several type Ia PSCs extending continuously over 5° in latitude and 5 km in altitude during January 1989. On occasion, type Ib clouds were observed adjacent to type Ia clouds; although smaller in scale, the type Ib clouds were

still characterized by a depth greater than 2 km and a horizontal extent greater than 200 km [*Browell et al.*, 1990]. More isolated regions of type II PSCs were also observed. During another campaign, the European Arctic Stratospheric Ozone Experiment (EASOE), an airborne lidar detected a pervasive type I PSC on December 11, 1991, that extended over 600 km in the horizontal and 5 km in the vertical [*Godin et al.*, 1994]. Using the lidar measurements of *Browell et al.* [1990], *Tabazadeh et al.* [1996] found that at locations where type Ia PSCs were observed, synoptic temperatures had been below the NAT frost point for at least a day, and they concluded that synoptic temperature histories could be used to predict the occurrence of type Ia PSCs. If the main criterion for type Ia PSC formation is synoptic in nature, then type Ia PSCs themselves would be expected to exist over synoptic scales. Indeed, a new analysis of the *Browell et al.* [1990] lidar observations (O. B. Toon, personal communication, 1997) indicates the presence of continuous type Ia PSCs over vast areas from January 6 to February 2, 1989, during AASE.

PSCs have also been detected through in situ measurements of aerosol particle size and volume. Large-scale PSCs, greater than 1000 km in horizontal extent at ~20 km, have been observed in AASE particle data [*Dye et al.*, 1990, 1992; *Kawa et al.*, 1992]. The data for one of these PSC encounters (January 24, 1989) have been found to be consistent with a type Ib cloud [*Drdla et al.*, 1994; *Carslaw et al.*, 1994; *Tabazadeh et al.*, 1994a]. Similarly, a flight on July 28, 1994, during the ASHOE campaign intercepted a 500-km-long portion of a PSC composed of ternary droplets near the vortex edge at ~20 km [*Dye et al.*, 1996; *Del Negro et al.*, 1997].

Thus evidence accumulated from remote and in situ measurements indicates that both type Ia (crystalline) and type Ib (liquid) PSCs routinely extend continuously over spatial scales comparable to or larger than the MLS FOV. Although, in principle, the change in gas-phase HNO_3 due to a very patchy NAT PSC could, when averaged over the MLS FOV, appear instead to indicate a cloud of ternary droplets, the weight of evidence suggests that this scenario is unlikely (although patches of type II PSCs smaller than can be resolved by MLS are likely to be embedded in large type I clouds, particularly in the Antarctic). For the purposes of this investigation we have assumed that the PSCs are uniform over the MLS FOV.

Another complicating factor in using the MLS HNO_3 measurements to investigate PSC composition, in addition to the limited precision and spatial resolution of the data, is that some critical quantities are not measured and must be estimated. Interpretation of the data is therefore predicated on a number of assumptions (which are discussed in detail in section 4). For these reasons, our results regarding PSC composition, while suggestive, are not conclusive.

4. Observations and Model Results

To date, MLS has observed six southern hemisphere winters: 1992–1997. However, problems with the UARS solar array caused the MLS instrument to be turned off during much of the early winter observing periods in both 1992 and 1995. In June 1995, UARS began operating in an instrument power sharing mode whereby MLS is periodically turned off; also at that time an MLS operational schedule consisting of (typically) 2 days of scanning followed by 1 day of "rest" was adopted to conserve the lifetime of the antenna scanning mechanism. The limited data coverage and the gaps in the data for these years are evident in Figure 1, which is discussed in more detail below. By the time of the 1997 early southern winter, the UARS power situation had degraded to the point that MLS measurements were collected on only 6 days during May and June; these data are not considered further here. Although they are presented briefly below, because of the short timescales involved, the sporadic data of 1992, 1995, and 1996 are not so well suited for a detailed study of PSC formation processes. In both 1993 and 1994, MLS obtained a complete set of daily limb scans during the early southern winter observing period. In this study we have chosen to examine the 1994 data more extensively for two reasons: the later onset of low temperatures and the earlier start of the observing period in 1994 (see Figure 1), capturing the initial stages of PSC formation, and the existence of data from the ASHOE campaign and the Polar Ozone and Aerosol Measurement (POAM) II instrument, providing supplementary information about environmental conditions in the polar vortex.

4.1. The 1994 Early Southern Winter

The behavior of MLS HNO_3 on selected days during the 1994 early southern winter south viewing period (May 24 to July 3) is shown in Plate 1. The MLS data are gridded by binning and averaging 24 hours of data and are then vertically interpolated to the 465-K potential temperature (θ) surface (ranging from ~30 to 60 hPa for the low temperatures inside the polar vortex) using United Kingdom Meteorological Office (UKMO) temperatures [*Swinbank and O'Neill*, 1994]. Contours of temperature and potential vorticity (PV) derived from the UKMO analyses are also shown. During southern late autumn and early winter (June–July), the lower stratospheric vortex is characterized by strong diabatic descent but very little latitudinal mixing across its boundary [*Manney et al.*, 1994]. In the absence of other effects, these conditions lead to large HNO_3 mixing ratios inside the vortex like those seen at the beginning of the observing period. The decreases observed in the HNO_3 abundances during winter are unlikely to be caused by dynamical processes and are attributed here to PSC activity. POAM II aerosol extinction measurements confirm the existence of PSCs during this time period [*Fromm et al.*, 1997].

Although 465-K temperatures have been below 195 K over a sizeable area since mid-May (see Figure 1), gas-phase HNO_3 values remain high in most regions of the vortex through the first week in June. A small pocket of low HNO_3 appears in the map on June 7 and intensifies as temperatures drop below 188 K the next day (not shown). Loss of gas-phase HNO_3 continues throughout the observing period, so that by the beginning of July very low HNO_3 concentrations

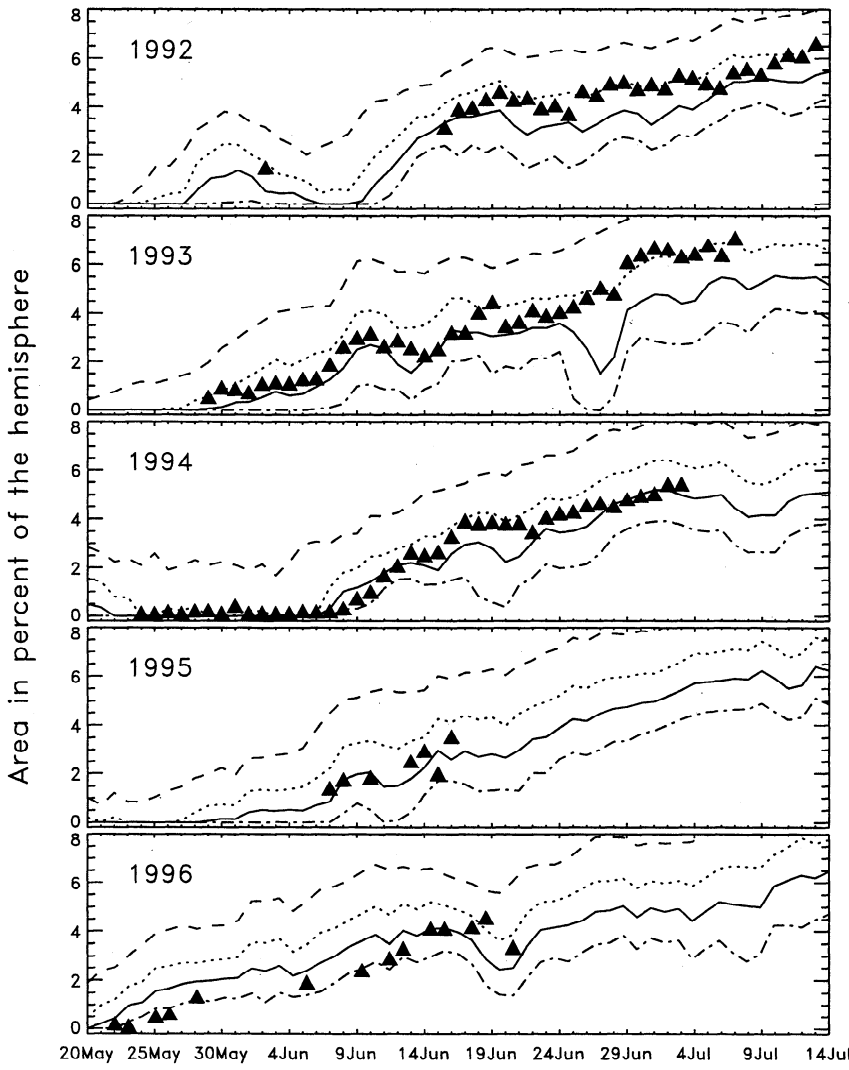

Figure 1. The area poleward of 60°S on the 465-K potential temperature surface (expressed as the percent of the hemisphere) as a function of time within which Microwave Limb Sounder (MLS) HNO_3 mixing ratios are below 4 ppbv (solid triangles) and United Kingdom Meteorological Office (UKMO) temperatures are below 188 K (dash-dotted lines), 190 K (solid lines), 192 K (dotted lines), and 195 K (dashed lines). Data for all five southern hemisphere early-winter south looking periods are shown. The solid triangles denote the days on which MLS performed full vertical scans in each year; data gaps in 1992, 1995, and 1996 are evident (see text).

(3 ppbv or less) are measured throughout the extensive cold region (not shown).

While maps constructed from gridded data provide a visually effective means of displaying observations, they can be deceptive in that the gridding process necessarily smoothes out the contributions from individual measurements. PSCs are confined to the cold regions, which in early winter can be fairly localized; given the spacing of the UARS orbit tracks, short-lived PSCs of limited geographical extent may be represented in only one or two MLS data points, or may go undetected altogether. In Plate 2a the retrieved HNO_3 mixing ratios for June 2 are shown again, this time only at the MLS measurement locations, and in Plate 2b the UKMO temperatures are shown interpolated to these locations. Relatively low HNO_3 mixing ratios are recorded for a few points where the temperatures are in the range 191–193 K. Although this area does register lower mixing ratios in the map of gridded data (Plate 1), the depression in HNO_3 in the low-temperature region is smaller than suggested by the individual measurements. In this study we mostly use averages of MLS data from several measurement locations rather than either individual observations (because of the noise associated with each retrieved profile; see section 2.2) or gridded data (because of the misrepresentation of small-scale features inherent in the gridding process). As discussed further below, the relationship between reductions in gas-phase HNO_3 and variations in temperature is also explored by binning the data with respect to temperature.

The vertical extent of severely depleted gas-phase HNO_3 and its relationship to low temperatures over the UARS

month are illustrated in Plate 3, which shows MLS HNO_3 as well as UKMO temperature and PV over the potential temperature range 420–585 K. The pink lines are contours of PV (scaled to yield similar values throughout the θ domain) that circumscribe the boundary of the vortex; the cyan and purple

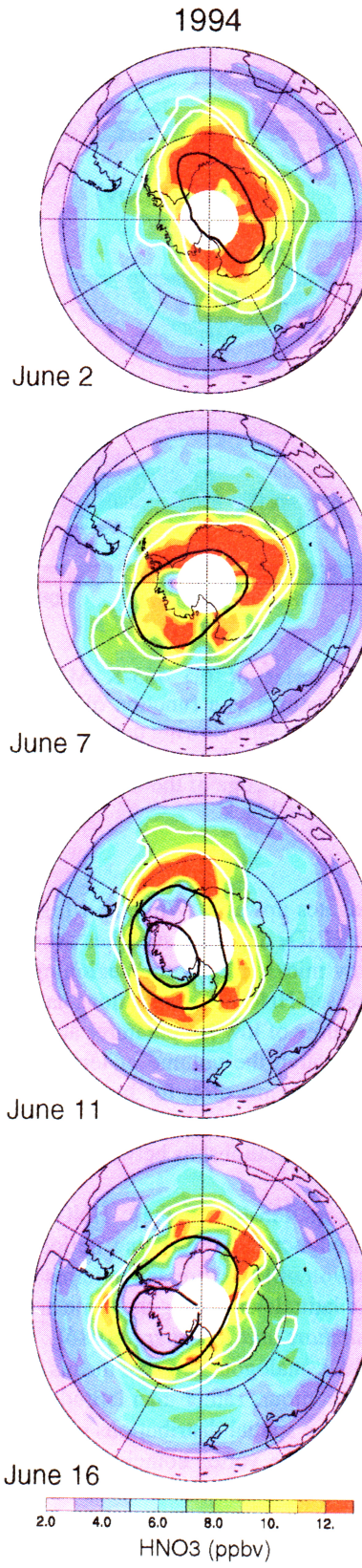

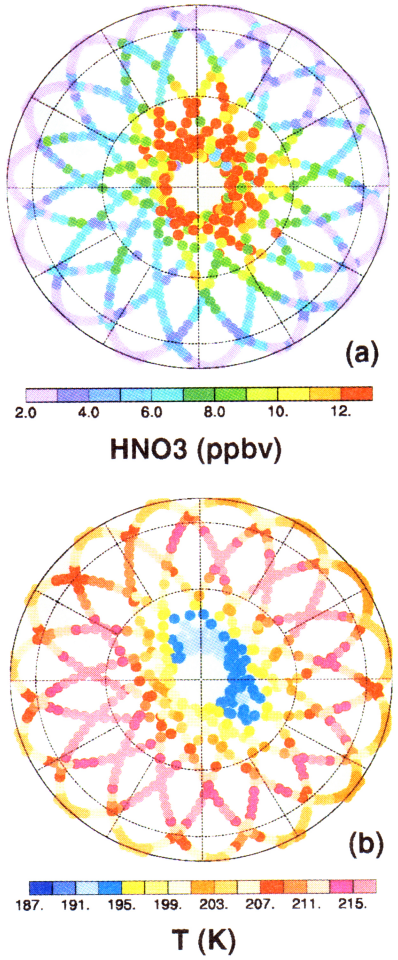

Plate 2. (a) The 465-K HNO_3 mixing ratios shown at the MLS measurement locations, with no horizontal binning or averaging performed, for June 2, 1994. (b) The 465-K UKMO temperatures for June 2, 1994, interpolated to the latitude/longitude coordinates of the MLS measurements.

lines demark the volumes within which the temperatures are below 192 K and the HNO_3 mixing ratios are below 4 ppbv, respectively. The surfaces of low HNO_3 along the perimeter of these plots are situated outside the vortex and are not associated with PSC formation. Temperatures in the upper

Plate 1. Maps of MLS HNO_3 (parts per billion by volume) for selected days during the 1994 early southern winter south viewing period, interpolated onto the 465-K potential temperature surface using UKMO temperatures. The maps are polar orthographic projections extending to the equator, with the Greenwich meridian at the top and with dashed black circles at 30°S and 60°S; blank spaces represent data gaps or bad data points. Superimposed in white are two contours of UKMO potential vorticity (PV): -0.25×10^{-4} K m^2 kg^{-1} s^{-1} (to represent the approximate edge of the winter polar vortex at this level) and -0.30×10^{-4} K m^2 kg^{-1} s^{-1} (a second contour to indicate the steepness of the PV gradient and thus the strength of the vortex). Superimposed in black are two contours of UKMO temperature: 195 K (the approximate existence threshold for type I polar stratospheric clouds (PSCs) and 188 K (the ice frost point).

portion of the vertical range are already well below 192 K by early June, but the bottom portion of the vortex does not cool below 192 K until June 8 (although 465-K temperatures are below 195 K at this time, as stated above). The HNO_3 depletion begins at the lowermost levels of the vortex and

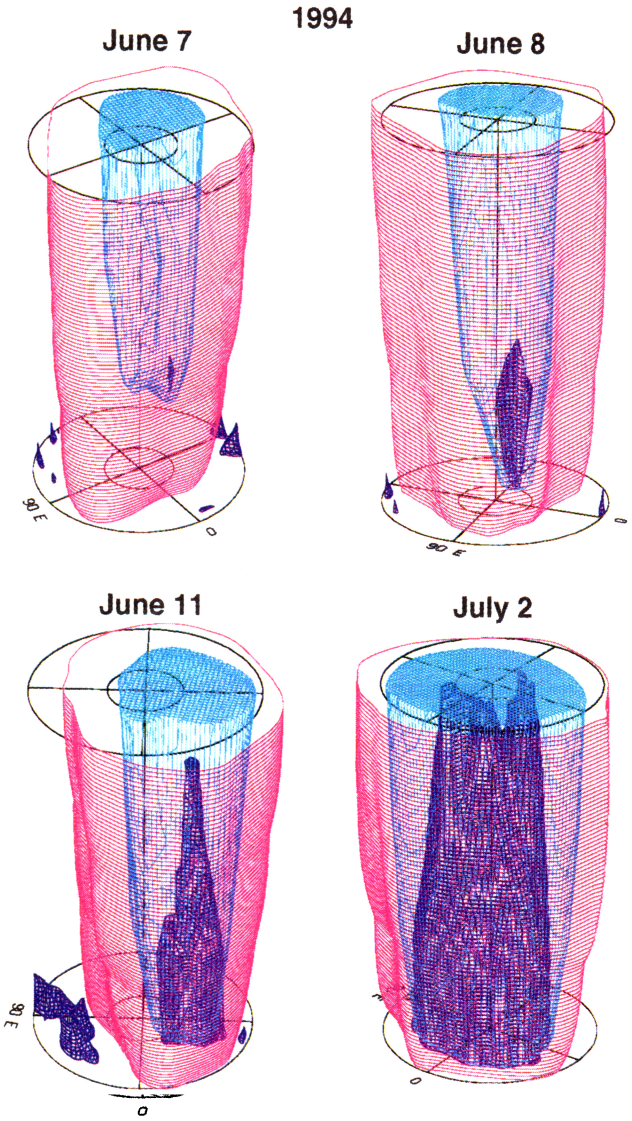

Plate 3. Plots illustrating the three-dimensional relationship between low temperature and severely reduced gas-phase HNO_3 inside the polar vortex for selected days during the 1994 early southern winter south viewing period. The vertical coordinate is potential temperature, ranging from 420 K to 585 K. Latitude circles are shown at 60°S and 80°S, and longitudes 0° and 90°E are labeled. The pink surface shows the 1.4 s^{-1} contour of scaled PV (corresponding to the -0.30×10^{-4} K m^2 kg^{-1} s^{-1} PV contour at 465 K [see *Manney et al.*, 1994]), which represents the approximate boundary of the polar vortex. The cyan surface shows the 192-K contour of UKMO temperature. The purple surface shows the 4-ppbv contour of MLS HNO_3. The surfaces of low HNO_3 along the perimeters of these plots are situated outside the vortex and are not associated with PSC formation; the geographic coverage of the HNO_3 plot is terminated at 60°S to minimize the presence of these surfaces. Different perspectives are used on each day to obtain the most unobstructed view of the vortex.

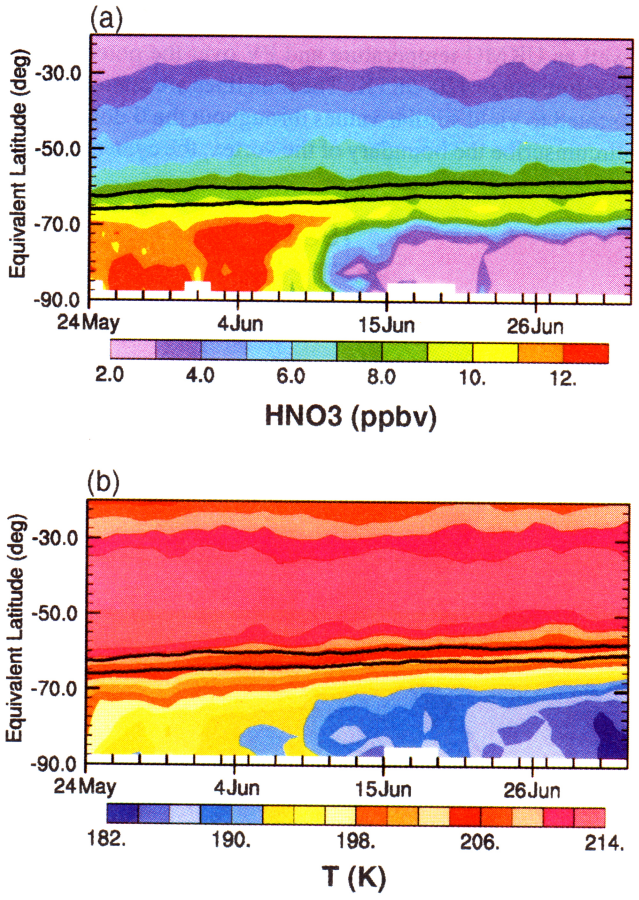

Plate 4. Time series of (a) 465-K MLS HNO_3 and (b) UKMO temperatures as a function of PV for the 1994 early southern winter south viewing period. PV is expressed in terms of equivalent latitude (see text). PV contours representing the approximate edge of the winter polar vortex (see Plate 1) are overlain in black.

gradually propagates upward. While still highly localized horizontally, the HNO_3 depletion stretches over a significant vertical extent by mid-June. By the beginning of July, the volume of depressed HNO_3 concentrations has expanded to nearly fill the volume of low temperatures at all but the topmost levels. Although the volume of temperatures below 188 K is smaller, the same plots for June 11 and July 2 using the 188-K temperature contour (not shown) indicate a substantially similar relationship between temperature and gas-phase HNO_3.

The evolution of 465-K gas-phase HNO_3 and UKMO temperatures throughout the observing period is shown in Plate 4 as a function of PV expressed in terms of equivalent latitude (i.e., the latitude enclosing the same area as a given PV contour [*Butchart and Remsberg*, 1986]). The quantities represented are analogous to zonal means but are calculated around PV contours rather than latitude circles. Both the temporal and the spatial distributions of reduced HNO_3 mixing ratios inside the vortex coincide closely with those of temperatures below 192 K. In contrast, the distribution of low HNO_3 does not correspond to that of temperatures below 195 K, the value commonly assumed as the threshold for PSC formation. The correlation in time between varia-

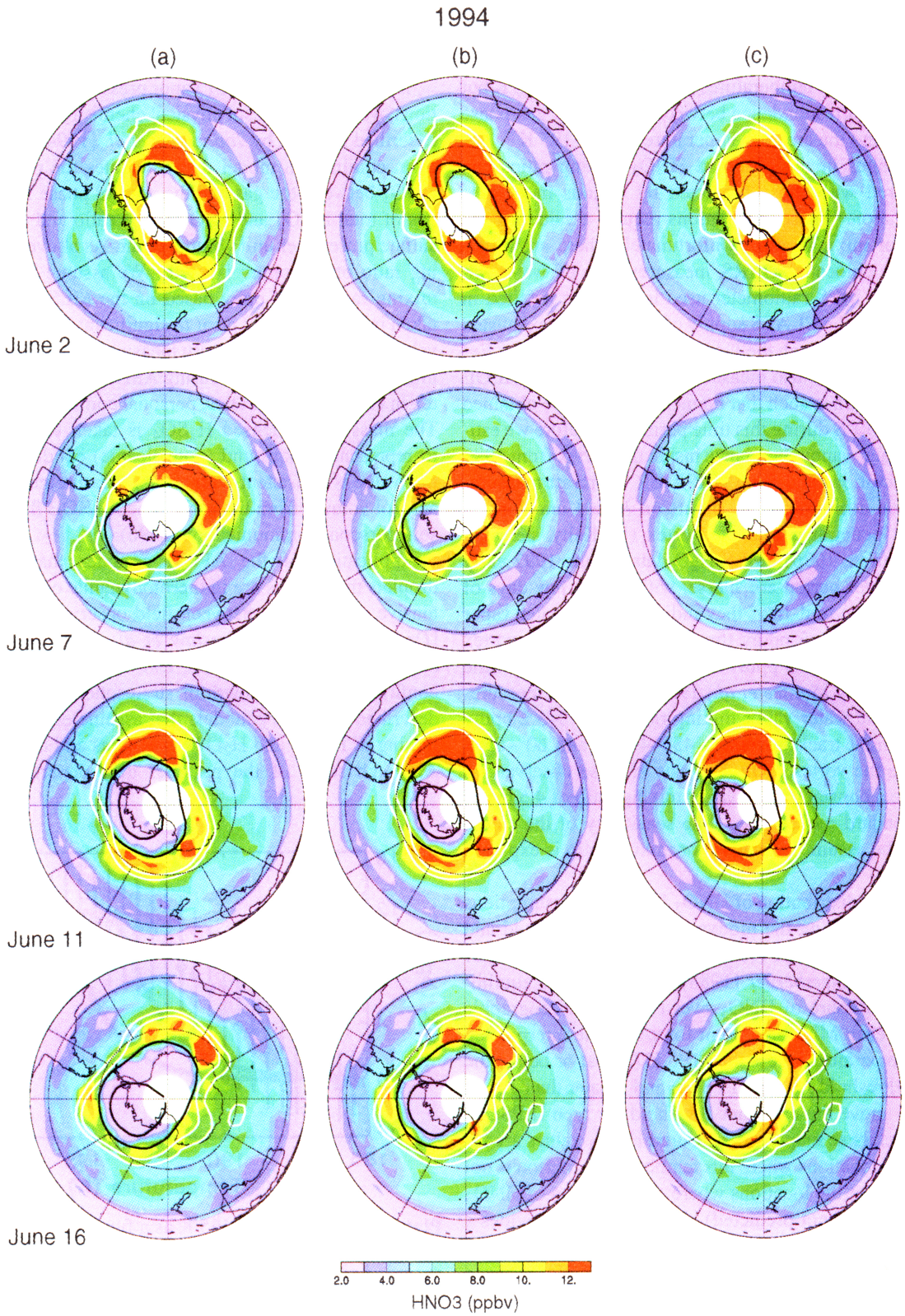

Plate 5. Maps at 465 K for the days during the 1994 early southern winter south viewing period shown in Plate 1, constructed from both MLS HNO_3 measurements and model calculations of the equilibrium vapor pressure of HNO_3 over (a) nitric acid trihydrate (NAT), using the formula of *Hanson and Mauersberger* [1988], (b) nitric acid dihydrate (NAD), using the formula of *Worsnop et al.* [1993], and (c) liquid ternary solutions, using the model of *Tabazadeh et al.* [1994b]. The maps are based on a H_2O mixing ratio of 4.5 ppmv and are constructed using the model values for HNO_3 inside the region where the temperature is between 186 K and 196 K and the MLS measurements of HNO_3 outside of this region.

tions in MLS HNO_3 mixing ratios and temperature fluctuations (noted for the 1995/1996 Arctic winter by *Santee et al.* [1996]) can also be seen in Figure 1. Again, there is a strong correspondence between the area of gas-phase HNO_3 loss and the area of temperatures in the range 190–192 K but only a weak correspondence between the area of gas-phase HNO_3 loss and the area of temperatures below 195 K.

The changes in the observed HNO_3 mixing ratios can be compared with those predicted by various models of PSC formation. These calculations require a value for the water vapor mixing ratio. Unfortunately, there are no simultaneous colocated UARS measurements of water vapor since the MLS radiometer used to measure it failed in April 1993 and the CLAES supply of cryogen was exhausted in May 1993. Although the UARS Halogen Occultation Experiment (HALOE) also measures water vapor, the HALOE observing pattern is such that no measurements are obtained poleward of 50°S during this time period. Therefore we estimate the water vapor abundance inside the vortex from 1992 MLS observations and from NASA ER 2 aircraft measurements made during ASHOE flights on June 1 and June 3, 1994, that penetrated into the vortex (K. Kelly, personal communication, 1996). MLS H_2O data for the 1992 early southern winter period are sparse, with only a few days of data in June and mid-July; they indicate initial water vapor mixing ratios of 4–5 ppmv throughout most of the vortex declining to less than 3 ppmv in the coldest regions near the pole by mid-July [*Santee et al.*, 1995]. The ER 2 measurements indicate water vapor mixing ratios of 5.0–5.2 ppmv along the flight track traversing 455–460 K and 60°–65°S (just inside the vortex). On the basis of these observations we assume a constant water vapor mixing ratio of 4.5 ppmv for the standard model runs. The sensitivity of the calculations to the assumed water vapor mixing ratio is explored below.

Maps of the distribution of HNO_3 for various assumptions about the controlling thermodynamics are constructed and compared with the data (Plate 5). We use the formula of *Hanson and Mauersberger* [1988] to calculate the equilibrium vapor pressure of HNO_3 over NAT at the geographic location of each MLS data point for which the interpolated UKMO temperature is less than 196 K (i.e., at or below the existence threshold for type I PSCs) and greater than 186 K (i.e., at or above the existence threshold for type II PSCs). To construct these maps, the measured HNO_3 values are retained at the locations where this temperature criterion is not satisfied (i.e., at the locations where sequestration of HNO_3 in type I PSCs is not predicted). This approach provides a picture of what MLS would have observed had NAT PSCs been forming according to the expression of *Hanson and Mauersberger* [1988]. Comparison of the maps in Plate 5a with those of MLS measurements in Plate 1 clearly shows that although temperatures are low enough to support NAT PSCs, they are not forming, at least not over spatial scales comparable to or larger than the ~400×100 km horizontal resolution of the MLS measurements. Similarly, we use the formula of *Worsnop et al.* [1993] to calculate the equilibrium vapor pressure of HNO_3 over NAD and construct the maps of Plate 5b. Although at first the spatial extent of low calculated mixing ratios is considerably larger than what is observed, by mid-June the NAD model provides fairly good agreement with the MLS HNO_3 data.

To determine the HNO_3 vapor pressure over ternary solutions, we use the aerosol physical chemistry model (APCM), described in detail by *Tabazadeh et al.* [1994b]. The APCM is an equilibrium model that calculates the partitioning of HNO_3 between the gas and the aerosol phase for given values of total HNO_3 and H_2O mixing ratio and total mass of sulfate present per unit volume of air. As above, a H_2O mixing ratio of 4.5 ppmv is used. We assume a total HNO_3 mixing ratio of 12 ppbv based on the MLS measurements taken inside the vortex prior to significant PSC activity. This value is consistent with in situ measurements of total reactive nitrogen (NO_y) obtained during ASHOE flights into the vortex in early June (D. Fahey, personal communication, 1996). The mass of condensed H_2SO_4 is taken to be 0.3 $\mu g/m^3$ to represent background (nonvolcanic) conditions. Again, this value is consistent with vortex measurements of sulfate aerosol volume from the early June ASHOE flights (J. Wilson, personal communication, 1996).

Application of the APCM assumes that the ternary droplets themselves are in thermodynamic equilibrium. Extensive comparisons between field observations and theory [*Drdla et al.*, 1994; *Carslaw et al.*, 1994; *Tabazadeh et al.*, 1994a; *Dye et al.*, 1996; *Del Negro et al.*, 1997] have confirmed that the growth of stratospheric aerosols is well described by ternary models that assume equilibrium partitioning of HNO_3 and H_2O between gas and aerosol phases. Although some of the particles may depart significantly

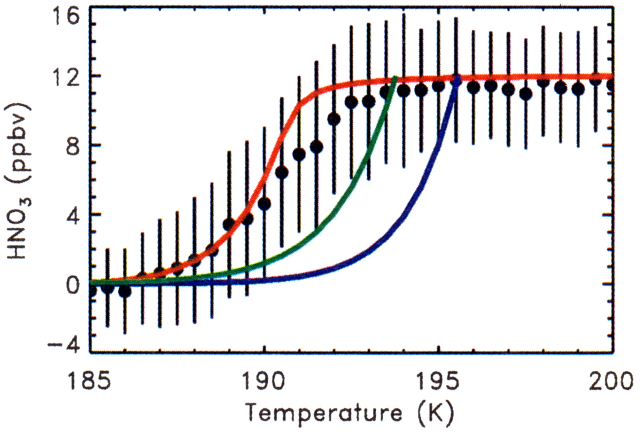

Plate 6. MLS HNO_3 at 465 K as a function of UKMO temperature for the 1994 early southern winter south viewing period. Approximately 8000 MLS data points inside the polar vortex (within the -0.30×10^{-4} K m^2 kg^{-1} s^{-1} contour of UKMO PV) were binned into 0.5-K temperature intervals and averaged (black circles; standard deviations are indicated by error bars). Also shown are the equilibrium vapor pressures of HNO_3 over NAT (blue line), NAD (green line), and liquid ternary solutions (red line) calculated assuming a H_2O mixing ratio of 4.5 ppmv, a total HNO_3 mixing ratio of 12 ppbv, and a sulfate mass loading of 0.3 $\mu g/m^3$ (background conditions).

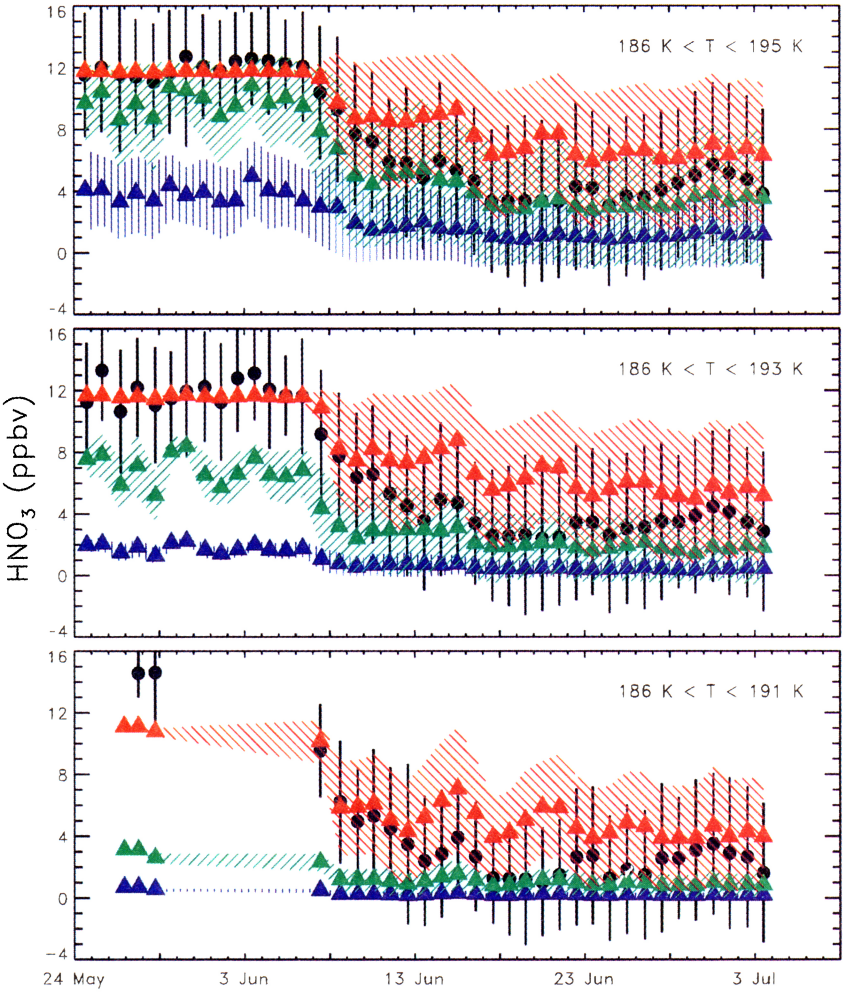

Plate 7. Time series (for the 1994 early southern winter south viewing period) of 465-K MLS HNO_3 (black circles) and calculated (see text for details) equilibrium vapor pressure of HNO_3 over NAT (blue triangles), NAD (green triangles), and ternary solutions (red triangles), averaged over the points enclosed within the annuli between the UKMO temperature contour of 186 K and the contours of 195, 193, and 191 K. The calculations were made using a total HNO_3 mixing ratio of 12 ppbv, a H_2O mixing ratio of 4.5 ppmv, and a sulfate mass loading of 0.3 $\mu g/m^3$ (background conditions). The standard deviations in the data averages are represented by the error bars, and the standard deviations in the model averages are indicated by the hatched areas.

from equilibrium, the overall aerosol volume matches that of the equilibrium ternary model very well, implying that the ternary system is not strongly influenced by the mesoscale temperature fluctuations [*Murphy and Gary*, 1995] that occur continuously in the stratosphere. Even under the rapid cooling conditions associated with lee wave events, while the smallest and the largest droplets are affected, the majority of the particles remain very close to the equilibrium composition [*Meilinger et al.*, 1995]. Therefore in this study we have assumed that if only liquid particles are present in an air mass, then the HNO_3 uptake can be accurately represented by an equilibrium ternary model.

Maps constructed from the MLS data and the ternary solution calculations are shown in Plate 5c. Comparison of Plates 5a–5c shows that NAT particles are the most efficient, and ternary droplets the least efficient, in depleting HNO_3 from the gas phase. The ternary solution calculations are in much closer (albeit not perfect) agreement with the MLS data during the first days of PSC formation. Eventually, however, the ternary model underestimates the spread of HNO_3 loss. For intermediate days such as June 11, the best match to the data would probably be provided by a nonequilibrium mixture of NAD (Plate 5b) and ternary (Plate 5c) aerosols.

The relationship between observed HNO_3 and temperature for the entire UARS month is compared to predictions from the NAT, NAD, and liquid ternary solution models in Plate 6. For this plot all of the 465-K MLS measurements obtained inside the polar vortex (approximately 8000 data points) were binned into 0.5-K temperature intervals and averaged (black circles, with the standard deviations represented by error bars). Despite the large amount of scatter in

the MLS data, it is clear that neither the NAT (blue line) nor the NAD (green line) models match the average behavior of the MLS HNO_3 over most of the temperature range. In contrast, the ternary solution model (red line) exhibits a temperature dependence similar to that of the MLS data, although it predicts too little gas-phase HNO_3 loss for temperatures between 190 K and 193 K. All three models converge to match the observations obtained at the lowest temperatures, which were mainly concentrated toward the end of the month.

A comparison of the changes in the observed and predicted HNO_3 values over time is presented in Plate 7. Averages of 465-K MLS HNO_3 (black circles, with the standard deviations represented by error bars) are calculated from points enclosed within the annuli between the 186-K temperature contour and the 195-, 193-, and 191-K temperature contours. The 186-K lower limit is imposed because no allowance is made for the formation of water ice particles. Toward the end of the observing period, the 186-K lower bound eliminates most of the low-HNO_3 points in the vortex interior and leads to increases in the averaged mixing ratios. For each data point within these temperature contours the equilibrium vapor pressure of HNO_3 over NAT, NAD, and ternary solutions is calculated as described above in connection with Plate 5. Averages of the model results are also calculated within the different annuli and are depicted by blue (NAT), green (NAD), and red (ternary solution) triangles. The standard deviations in the model averages are indicated by the hatched areas.

The assumption of a NAT composition for PSCs leads to very low HNO_3 vapor concentrations that are inconsistent with the MLS observations from late May and early June. The NAD model predicts HNO_3 values that match the data closely during the latter half of the observing period; although the initial trend for NAD is similar to that seen in the data for the 195-K contour average, agreement with the data is much poorer for the averages at lower temperatures. In contrast, the behavior predicted for a ternary solution composition is in good agreement with the data during the early stages of HNO_3 depletion for all three temperature contour averages, with the best agreement attained at the lowest temperatures. Comparison of Plate 7 and Figure 2 shows that significant incorporation of HNO_3 into the ternary solution aerosols does not occur until the average temperatures drop below ~192 K.

Interpretation of the MLS data on the 465-K isentropic surface is potentially complicated by the processes of denitrification, whereby large PSC particles remove HNO_3 through gravitational settling out of the layer, and renitrification, whereby particles falling from above enhance HNO_3 through evaporation in the layer. Although various scenarios have been proposed in which denitrification takes place independent of the formation of water ice clouds [*Salawitch et al.*, 1989; *Toon et al.*, 1990b; *Murphy and Gary*, 1995], in general, the most intense denitrification is expected to be accompanied by dehydration. Since we have omitted from our analyses those regions where type II PSC formation is possible, the effects of severe denitrification have been largely eliminated. However, transport processes in the vortex lead

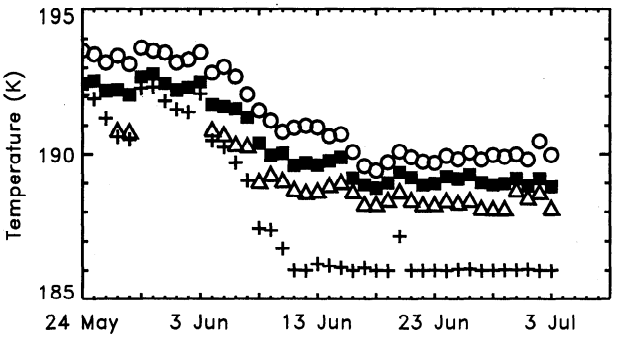

Figure 2. Time series (for the 1994 early southern winter south viewing period) of 465-K UKMO temperatures averaged over the annuli between the temperature contours of 186 K and 195 K (open circles), 193 K (solid squares), and 191 K (open triangles). Also shown are the minimum 465-K UKMO temperatures within those regions (plus signs; note that the minimum temperatures within the vortex as a whole, which are not shown, are much lower).

to dilution of the high HNO_3 concentrations in unperturbed regions as denitrified air is mixed in. To estimate the impact of denitrification on the total HNO_3 available in the PSC-free portions of the vortex, daily averages of HNO_3 are calculated from points located inside the vortex but outside the regions where HNO_3 mixing ratios are below 10 ppbv. These averaged HNO_3 values (not shown) exhibit a decrease of ~1.5 ppbv over the course of the observing period. Slightly larger decreases are obtained when averages are calculated over regions bounded by smaller HNO_3 mixing ratios (e.g., ~2.5 ppbv for a HNO_3 cutoff value of 4 ppbv). Because of the long timescale for HNO_3 photolysis during polar winter in the lower stratosphere [e.g., *Austin et al.*, 1986], the decline in these averaged HNO_3 values probably arises mainly from denitrification. The ternary model is very sensitive to the total amount of HNO_3. Lower abundances of available HNO_3 (e.g., ~6–8 ppbv, rather than 12 ppbv as in Plate 7; not shown) brought about by denitrification would improve the agreement between the ternary model and the observations toward the end of the observing period. However, the ternary droplets themselves are relatively small in size [e.g., *Toon et al.*, 1990a] and are unlikely to cause significant denitrification, especially not in the short period of time over which the best agreement with the measurements switches from the ternary to the NAD model (see Plate 7). Unlike the ternary model, the NAD predictions are not strongly dependent on the total HNO_3. Although the ternary model could be made to match the data well throughout the entire observing period by invoking either rapid denitrification or rapid HNO_3 photolysis, a more likely explanation of the behavior depicted in Plate 7 involves a change of phase from ternary solutions to NAD.

Temperatures in the layers above 465 K are low enough for type I and, in the latter half of the study period, type II PSC formation. Evidence of the vertical redistribution of HNO_3 through evaporation of falling PSC particles has been seen in both hemispheres [*Arnold et al.*, 1989; *Hübler et*

al., 1990; *Hofmann and Deshler*, 1991; *Kawa et al.*, 1992; *Tuck et al.*, 1995]. In these cases, however, HNO_3 enhancement was observed at much lower levels in the atmosphere. Renitrification requires evaporation to halt particle sedimentation and liberate gas-phase HNO_3. Temperatures at 465 K remain below the NAT existence threshold in much of the vortex throughout this UARS month. Therefore any PSC particles that form at higher altitudes and are large enough to undergo gravitational settling would likely pass through the 465-K level without evaporating.

Another process affecting HNO_3 abundances in the lower stratosphere is diabatic descent. Results from a three-dimensional Lagrangian transport calculation (not shown) similar to those described by *Manney et al.* [1995a] indicate that descent leads to an increase in vortex-averaged HNO_3 at 465 K of ~0.5 ppbv over the 30 days between June 2 and the end of the observing period. However, the calculations show essentially no change in HNO_3 when averages are limited to the low-temperature areas. The differences between the two sets of averages reflect the fact that descent during early southern winter is stronger along the vortex edge than in its interior [*Manney et al.*, 1994], where the cold regions are predominantly confined. In any case, vertical transport produces only small increases in the HNO_3 mixing ratios at 465 K during this UARS month. Since these increases are offset by the effects of denitrification and HNO_3 photolysis discussed above, we do not consider them further.

Of greater importance in interpreting the MLS HNO_3 measurements are the uncertainties associated with various model parameters. One means of assessing these uncertainties is to explore a range of parameter values in performing the model calculations of Plate 7. Plate 8, discussed below, illustrates the sensitivity of the model calculations to the assumed water vapor mixing ratio, the temperature, and the assumed sulfate aerosol loading. For all cases shown, the averages are calculated from points enclosed within the annulus between the 186-K and 195-K temperature contours using a total HNO_3 mixing ratio of 12 ppbv; these results can be compared with those of the top panel of Plate 7. In general, the model calculations exhibit much less sensitivity for averages computed within the 191-K temperature contour.

Model calculations were performed for a series of water vapor mixing ratios using the nominal UKMO temperatures and background aerosol conditions. Results for the extremes of 3 and 6 ppmv are shown in Plate 8a since they bracket the behavior of the predicted HNO_3. Although the MLS data indicate water vapor mixing ratios on the order of 3 ppmv by mid-July, they do not support such extensive water vapor loss in the late May/early June time frame [*Santee et al.*, 1995]. Nevertheless, the top panel of Plate 8a shows that the agreement of both the NAT and NAD models with the data could be significantly better than that of the standard run if we have overestimated the water vapor abundance. In the case of water mixing ratios larger than those of our standard run, the bottom panel of Plate 8a shows even better agreement between the data and the ternary solution model.

We also investigate the influence of possible temperature biases on the model results. Differences between the UKMO analyses and radiosonde observations at 50 hPa at high southern latitudes during May and June are typically within about ± 1 K, with even smaller systematic biases (<0.5 K) indicated [*Manney et al.*, 1996]. Varying the temperature by ± 1 K from the nominal UKMO value at each point yields results (not shown) in which the ternary and NAD models exhibit a similar level of agreement with the data, but the NAT model still significantly overestimates the HNO_3 depletion throughout the observing period. Results from the more extreme case of varying the temperature by ± 3 K from the nominal UKMO value at each point are shown in Plate 8b (for a total water vapor mixing ratio of 4.5 ppmv and background aerosol conditions). Note that shifting the temperature by this amount at each point causes a different set of measurements to be enclosed within the annulus between the 186-K and 195-K temperature contours, resulting in data averages much different from those of Plate 7. Although differences between UKMO and radiosonde temperatures of this magnitude occur only occasionally during this time period, Plate 8b shows that if the UKMO temperatures are systematically biased high by 3 K (top panel), then the discrepancy between the data and the NAT and NAD models is greater than indicated by the standard run, whereas the ternary model provides a fairly good match to the data throughout the entire month; if the UKMO temperatures are systematically biased low by 3 K (bottom panel), then the agreement of NAT with the data is improved over that of the standard run, particularly during the latter half of the period. Note that comparisons of UKMO and radiosonde observations [*Manney et al.*, 1996] do not support the existence of systematic biases larger than ~1 K at any time during the southern hemisphere winter and suggest that systematic biases are even smaller in May and June.

In Plate 8c the sulfate mass is varied between 3 and 30 $\mu g/m^3$ (using the nominal UKMO temperatures and a total water vapor mixing ratio of 4.5 ppmv). Although unaffected by the sulfate aerosol loading, the NAT and NAD model curves are retained for consistency. Enhancement of the total sulfate mass leads to greater uptake of gas-phase HNO_3, as shown previously by *Carslaw et al.* [1994] and *Tabazadeh et al.* [1994b]. The bottom panel of Plate 8c represents strongly perturbed volcanic conditions; the top panel shows that if we have underestimated the residual effects from the Mount Pinatubo eruption, then the agreement of the ternary model with the data could be worse at the beginning of the observing period than indicated by the standard run.

Finally, in Plate 8d we explore the potential impact on the model comparisons of bias errors in the MLS HNO_3 measurements. The model calculations are made using the standard values (H_2O = 4.5 ppmv, total HNO_3 = 12 ppbv, sulfate mass = 0.3 $\mu g/m^3$) as in Plate 7, but the MLS data are shifted by ± 2 ppbv at each measurement location. Plate 8d shows that if the HNO_3 retrievals interpolated to 465 K are biased high by 2 ppbv (top panel), then the agreement with the NAD model is considerably better than indicated by the results of Plate 7. On the other hand, a low bias of 2 ppbv in

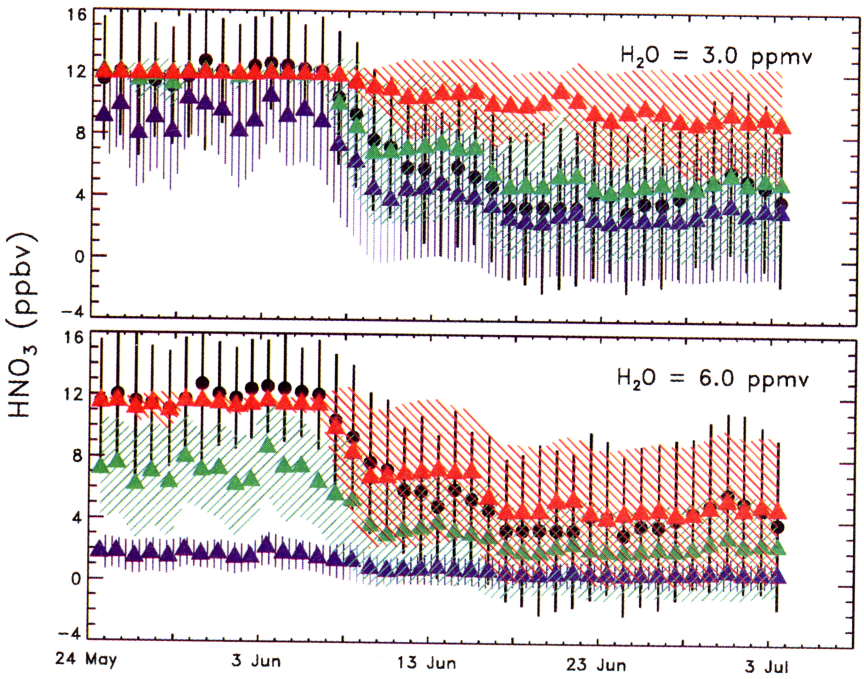

Plate 8a. Time series, as in Plate 7, to illustrate the sensitivity of the HNO_3 vapor pressure calculations to the assumed water vapor mixing ratio, which is varied between 3 and 6 ppmv. The averages are calculated from points enclosed within the annulus between the 186-K and 195-K temperature contours using a total HNO_3 mixing ratio of 12 ppbv.

the MLS data (bottom panel) would point to an even greater discrepancy between the data and the NAT and NAD models. Further validation efforts to quantify any bias errors in the MLS HNO_3 data are currently underway.

That the data are matched better by a ternary solution model during the initial stages of PSC formation but as time progresses are matched better by a NAD model is consistent with a scenario proposed by *Tabazadeh et al.* [1994a, 1995, 1996] based on analysis of aircraft data. According to this scenario, ternary solutions form in air masses in which the background sulfate aerosols are liquid (e.g., in the first cooling cycles) and the temperatures have recently dropped a few

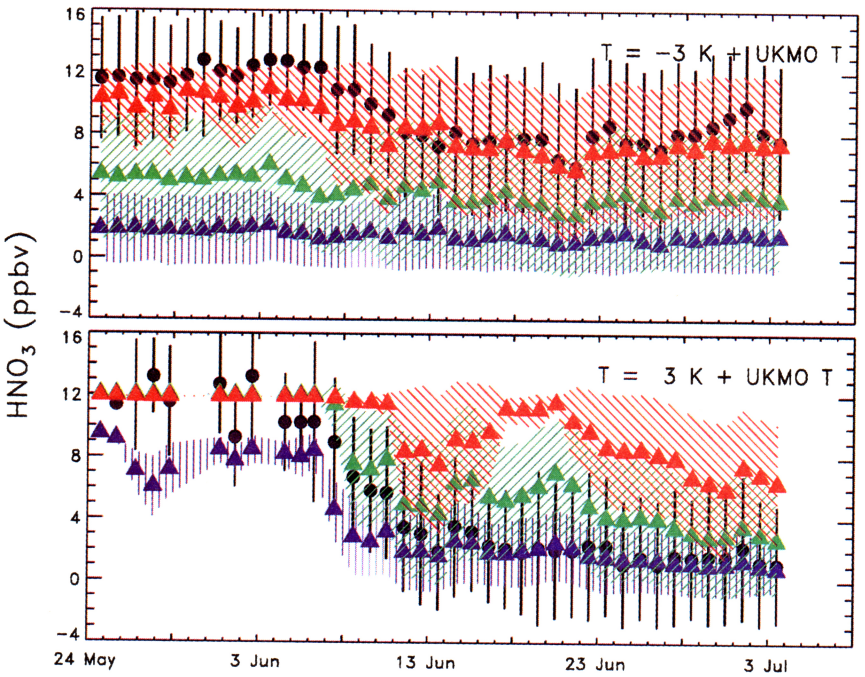

Plate 8b. Same as in Plate 8a, but for the temperature, which is varied by ±3 K from the nominal UKMO temperature at each measurement location.

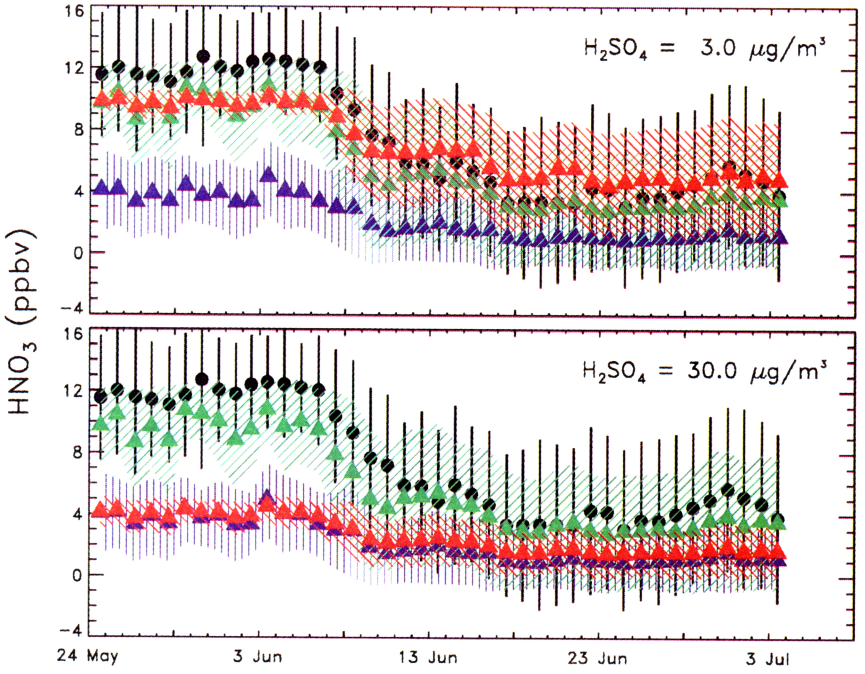

Plate 8c. Same as in Plate 8a, but for the assumed total sulfate mass, which is varied between 3 and 30 $\mu g/m^3$.

degrees below the NAT condensation point. After exposure to low temperatures for more than ~1 day, NAT or NAD particles begin to nucleate, and a mixed cloud results while a transfer of HNO_3 vapor from the ternary solution droplets to the more stable crystalline particles takes place, with eventual complete conversion. That is, a nonequilibrium situation arises after some of the ternary droplets freeze, and the HNO_3 vapor pressure, initially at the ternary limit, gradually decreases as the HNO_3 is transferred to the thermodynamically more favorable NAT or NAD particles. The MLS observations (see Plate 7) suggest that the first crystalline structure to form is NAD, the preferential nucleation and persistence of which was first propounded for the polar stratosphere by *Worsnop et al.* [1993]. In addition, the

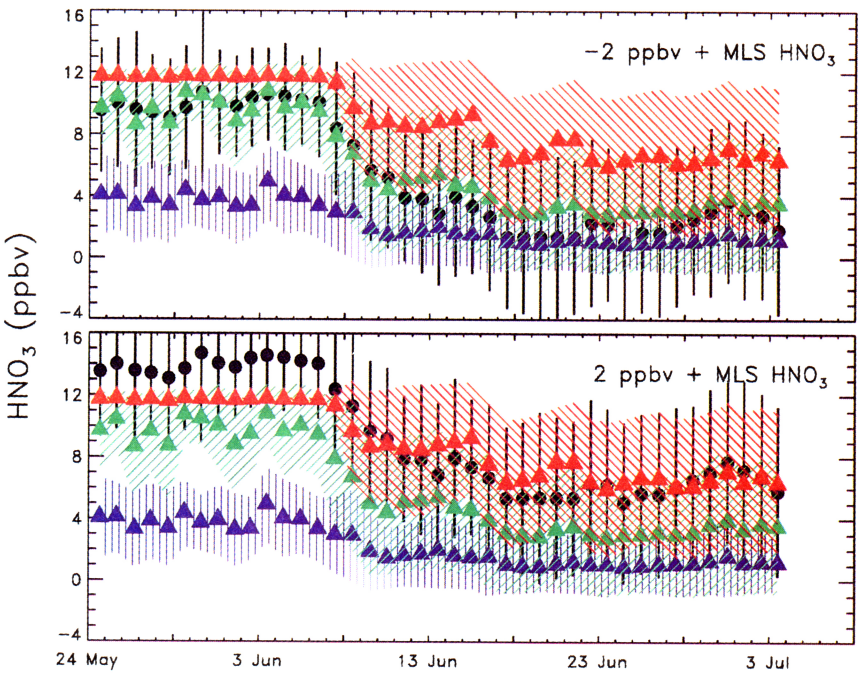

Plate 8d. Time series, as in Plate 7, to explore the potential impact on the model comparisons of bias errors in the MLS HNO_3, which is varied by ±2 ppbv from the nominal mixing ratio at each measurement location. Model calculations are made using the standard parameter values as in Plate 7.

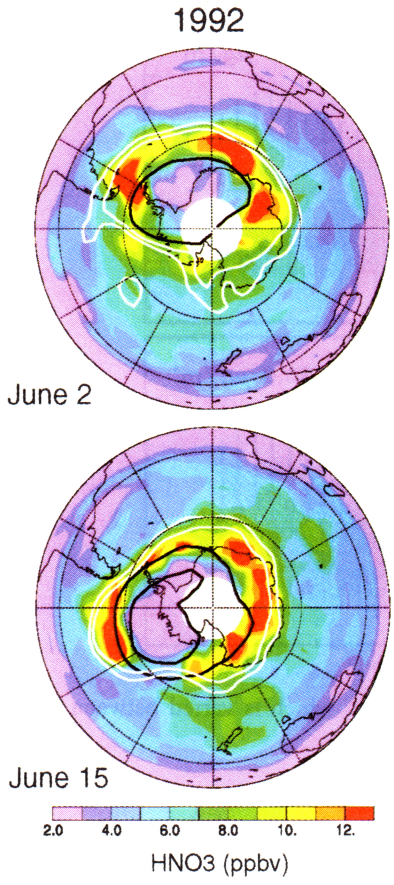

Plate 9. Same as in Plate 1, but for the 1992 early southern winter south viewing period.

MLS data indicate that the conversion of ternary solutions to NAD occurs more slowly (spanning at least several days) than suggested by *Tabazadeh et al.* [1996].

This scenario is also supported by the analyses of *Larsen et al.* [1996, 1997]. They examined balloon-borne backscatter measurements from several Arctic winters, along with back trajectory calculations, and found that ternary solutions were observed predominantly in air masses that were in the process of undergoing relatively fast cooling, whereas most solid type Ia PSCs exhibiting the characteristics of NAT had aged at temperatures below the NAT condensation point for more than 1–2 days. In addition, *Dye et al.* [1996] reported that particle volumes observed at the lowest temperatures during the ASHOE PSC encounter were not entirely consistent with an equilibrium ternary model, and they suggested a mixture of ternary droplets with NAT or other solid phases. In section 5 we use trajectory calculations to further investigate the evolution of the PSC composition.

4.2. The 1992 Early Southern Winter

At the start of the 1992 early southern winter south viewing period on June 2 (Plate 9), HNO_3 abundances are high in the portion of the vortex where temperatures are above ~195 K, due to diabatic descent as discussed above. However, a deficit in gas-phase HNO_3 is apparent inside most (but not all) of the region where temperatures are below ~195 K, more or less conforming to the pattern expected for crystalline type I PSCs. These observations are in contrast to the large HNO_3 mixing ratios observed throughout most of the vortex, including the low-temperature region, in early June 1994 (see Plate 1 and Figure 1). Operational constraints precluded the acquisition of additional data during 1992 until June 15 (Plate 9), by which time temperatures over a broad region have dropped below 188 K, and HNO_3 maps for the two years appear substantially similar.

The difference in the behavior of MLS HNO_3 during early June in 1992 as compared with 1994 is probably related to the sulfate aerosol loading following the eruption of Mount Pinatubo [e.g., *Tabazadeh et al.*, 1994b; *Carslaw et al.*, 1994]. *Russell et al.* [1996] have shown that the stratospheric particle optical depth in April 1992 at 60°S–70°S was enhanced by roughly a factor of 20–30 over pre-Pinatubo levels. In Plate 10 we show HNO_3 maps con-

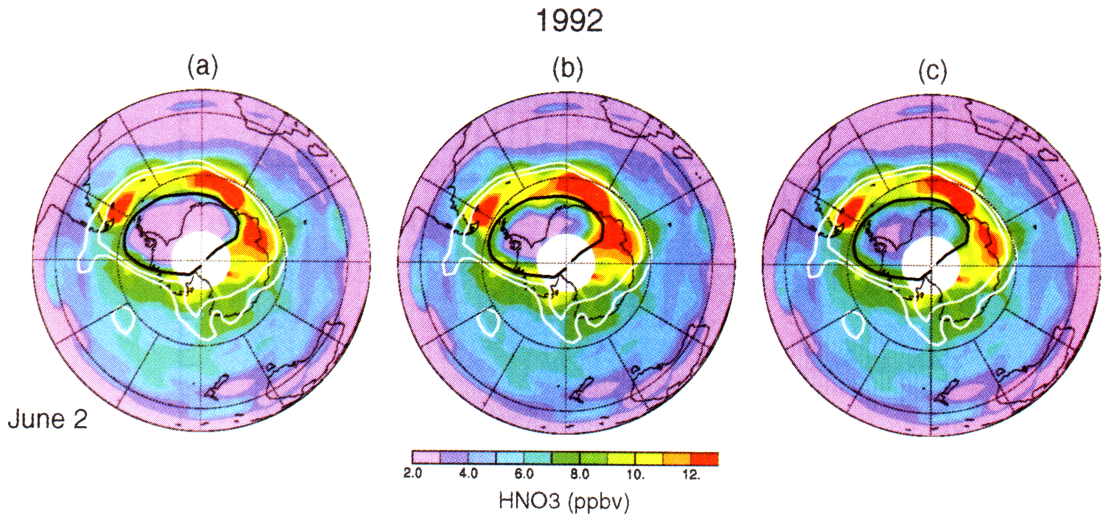

Plate 10. Same as in Plate 5 for (a) NAT, (b) NAD, and (c) liquid ternary solutions (using a total sulfate mass of 10 $\mu g/m^3$), for June 2, 1992.

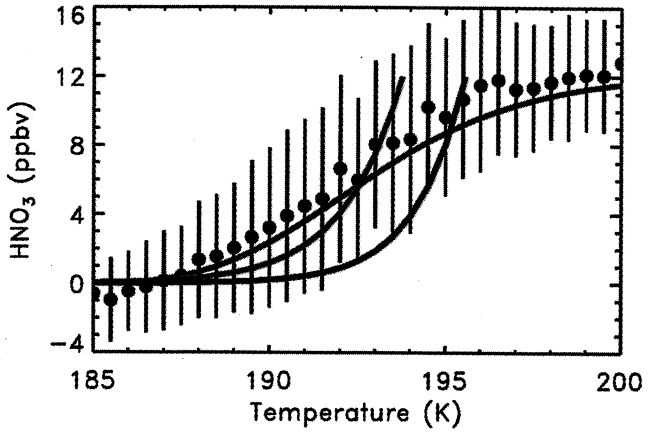

Plate 11. Same as in Plate 6, but for the 1992 early southern winter south viewing period. The averages represent approximately 6300 MLS data points inside the polar vortex. The ternary model curve was calculated using a sulfate mass loading of 10 $\mu g/m^3$ to account for the Pinatubo enhancement.

structed for June 2 from the MLS data and the various PSC composition models using a H_2O mixing ratio of 4.5 ppmv and a total HNO_3 mixing ratio of 12 ppbv, as discussed in connection with Plate 5, and a total sulfate mass of 10 $\mu g/m^3$ to represent the Pinatubo enhancement. Although the ternary model significantly underestimates the HNO_3 uptake for sulfate mass loadings of 0.3 $\mu g/m^3$ and 3 $\mu g/m^3$ (not shown), it agrees fairly well with the data for a sulfate mass of 10 $\mu g/m^3$. However, the models constrained by the thermodynamics of NAD and NAT also agree reasonably well with the observed HNO_3. The single MLS observation day at the beginning of the 1992 early southern winter study period does not allow us to definitively distinguish between any of the compositions. However, the temperature dependence of the HNO_3 measurements obtained inside the polar vortex during the course of the observing period, shown in Plate 11, indicates that a ternary solution model using a sulfate mass of 10 $\mu g/m^3$ predicts reductions in gas-phase HNO_3 similar to those observed by MLS.

4.3. The 1993 Early Southern Winter

As in 1994, MLS obtained a complete set of daily limb scans during the 1993 early southern winter south looking period (May 29 to July 7; selected days shown in Plate 12). Unlike in 1994, however, in 1993, MLS did not resume south viewing in time to capture the incipient stage of PSC formation. As indicated in Figure 1, the areal extent of HNO_3 mixing ratios below 4 ppbv measured on the first day of the 1993 observing period is not achieved in 1994 until approximately June 9, midway through that observing period. The relationship between low HNO_3 and low temperature for these days is different for the two years: In 1993, the areal extent of low HNO_3 values is comparable to that of temperatures below 192 K, but in 1994 it is much smaller. In fact, in 1994 the areal extent of low HNO_3 remains smaller than that of temperatures below 190 K for several days. A possible explanation for this difference is the lingering aftereffects in 1993 of the eruption of Mount Pinatubo. *Russell et al.* [1996] have shown that the stratospheric particle optical depth in April 1993 at 60°S to 70°S was still enhanced by roughly a factor of 10 over pre-Pinatubo levels. Equilibrium calculations

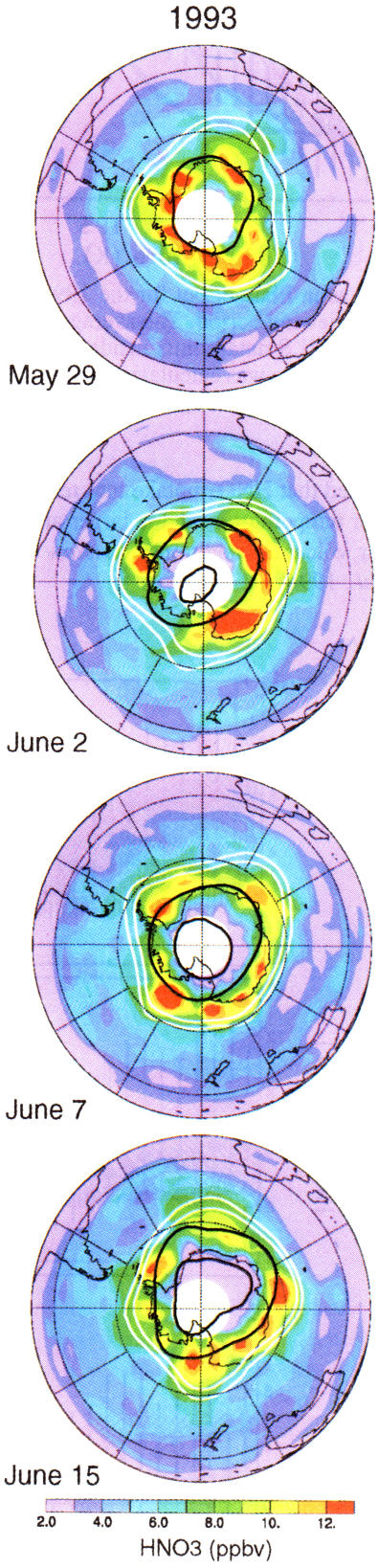

Plate 12. Same as in Plate 1, but for the 1993 early southern winter south viewing period.

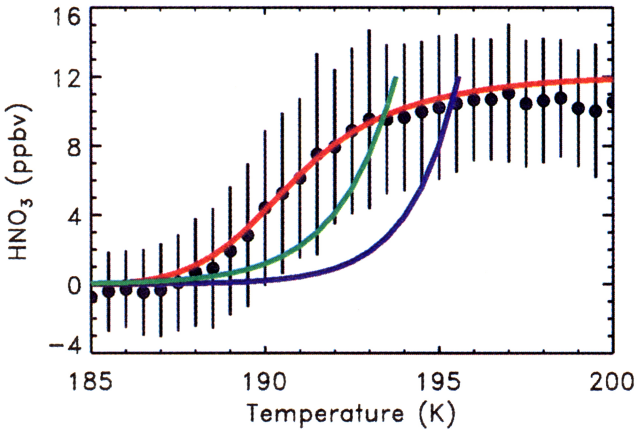

Plate 13. Same as in Plate 6, but for the 1993 early southern winter south viewing period. The averages represent approximately 8500 MLS data points inside the polar vortex. The ternary model curve was calculated using a sulfate mass loading of 3 $\mu g/m^3$ to account for the residual Pinatubo enhancement.

have demonstrated that HNO_3 uptake into ternary solutions occurs at higher temperatures, and is larger at a given temperature, under volcanic conditions [*Carslaw et al.*, 1994; *Tabazadeh et al.*, 1994b].

The HNO_3/temperature relationship inside the vortex for this observing period (Plate 13) shows that a ternary solution model using a total sulfate mass of 3 $\mu g/m^3$ to account for the residual Pinatubo enhancement agrees well with the MLS data. In Plate 14 the changes over time in the observed HNO_3 mixing ratios are compared with those predicted by the various PSC composition models (using a H_2O mixing ratio of 4.5 ppmv, a total HNO_3 mixing ratio of 12 ppbv, and a total sulfate mass of 3 $\mu g/m^3$). As was seen for the 1994 data, the NAT model severely underestimates the observed HNO_3 abundances, while the NAD model calculations match the data closely in the latter half of the observing period and the ternary model provides excellent agreement initially.

Comparison of Plate 14 with Plate 7 reveals that the ternary calculations provide a good description of the data after PSC formation begins for a much longer duration in 1993 than in 1994. This is probably related to the significant differences in composition between ternary solutions formed under volcanic conditions and those formed under background aerosol conditions [*Tabazadeh et al.*, 1994b]. These compositional differences during volcanically perturbed periods may give rise to changes in the NAT or NAD saturation ratio that hamper the formation of crystalline PSCs from the

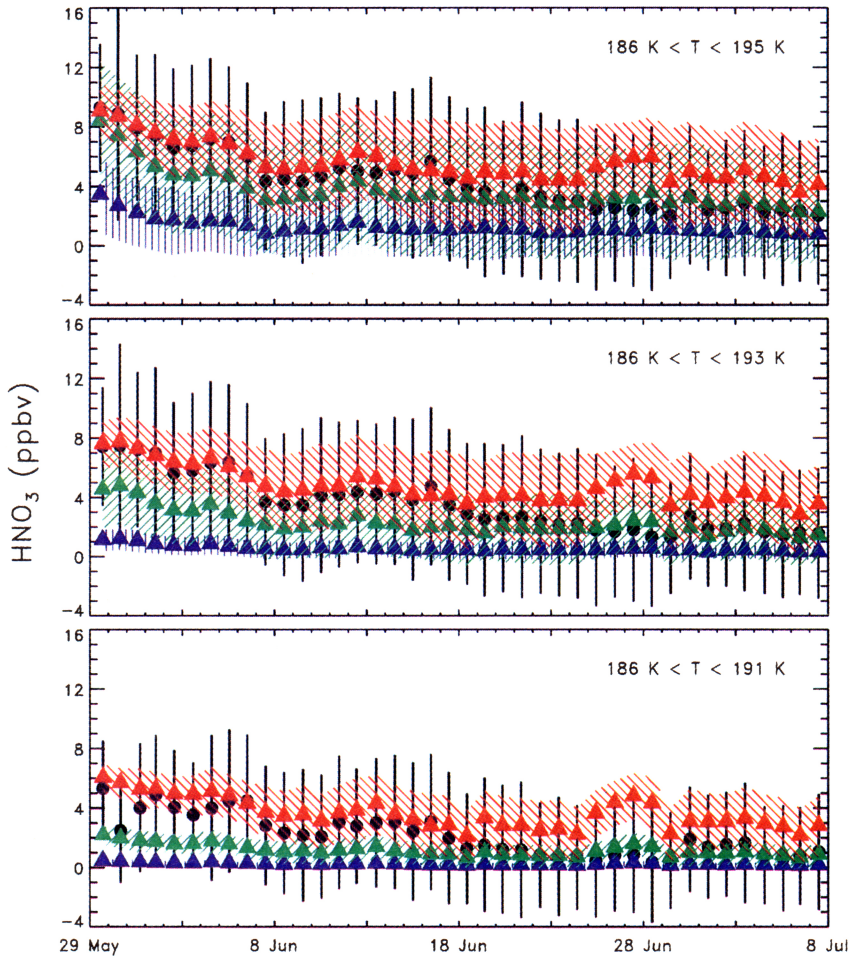

Plate 14. Same as in Plate 7, but for the 1993 early southern winter south viewing period, using a total HNO_3 mixing ratio of 12 ppbv, a H_2O mixing ratio of 4.5 ppmv, and a total sulfate mass of 3 $\mu g/m^3$.

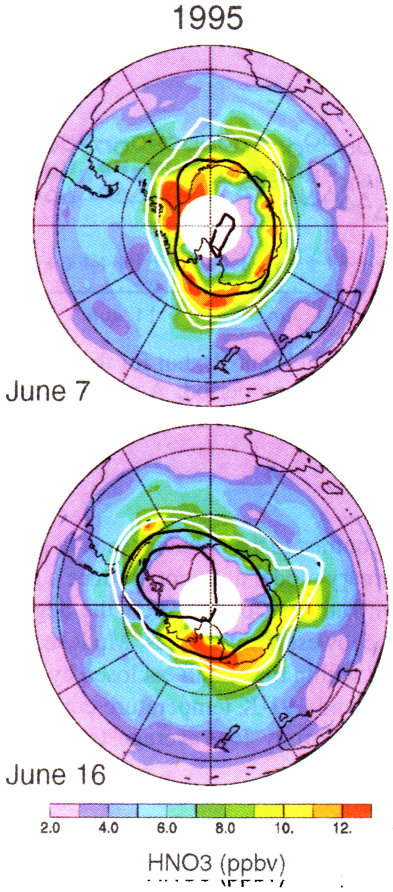

Plate 15. Same as in Plate 1, but for the 1995 early southern winter south viewing period.

ternary solutions. Plate 14 suggests, however, that the conversion to NAD did eventually take place in 1993.

4.4. The 1995 Early Southern Winter

The first and last days for which MLS data are available during the 1995 early southern winter are June 7 and June 16, respectively (Plate 15). Figure 1 shows that in 1995 temperatures have been below 190 K since the beginning of June, and by the first day of MLS observations there is already a substantial area of low HNO_3 mixing ratios. Again, MLS has not observed the onset of PSC formation. Although the NAD model produces HNO_3 depletion over too broad an area, especially for the first few days of measurements, it still provides the best agreement with the MLS data (not shown).

4.5. The 1996 Early Southern Winter

During the 1996 early southern winter the lower stratosphere was substantially colder than average [*Climate Prediction Center*, 1996], with 465-K minimum temperatures continuously below 195 K after May 7 and 188 K after May 22. The earlier onset and greater area of very low temperatures in the 1996 early winter is evident in Figure 1. Because of UARS power limitations, MLS measurements are not available during this period until May 22, by which time PSC formation has already begun (Plate 16). Although the progression of HNO_3 depletion appears similar for 1996 and 1994, its relationship with low temperature is not: Initially, the extent of the reduction in gas-phase HNO_3 within the regions of lowest temperature is smaller in 1996 than in 1994. In fact, Figure 1 shows that despite the very low temper-

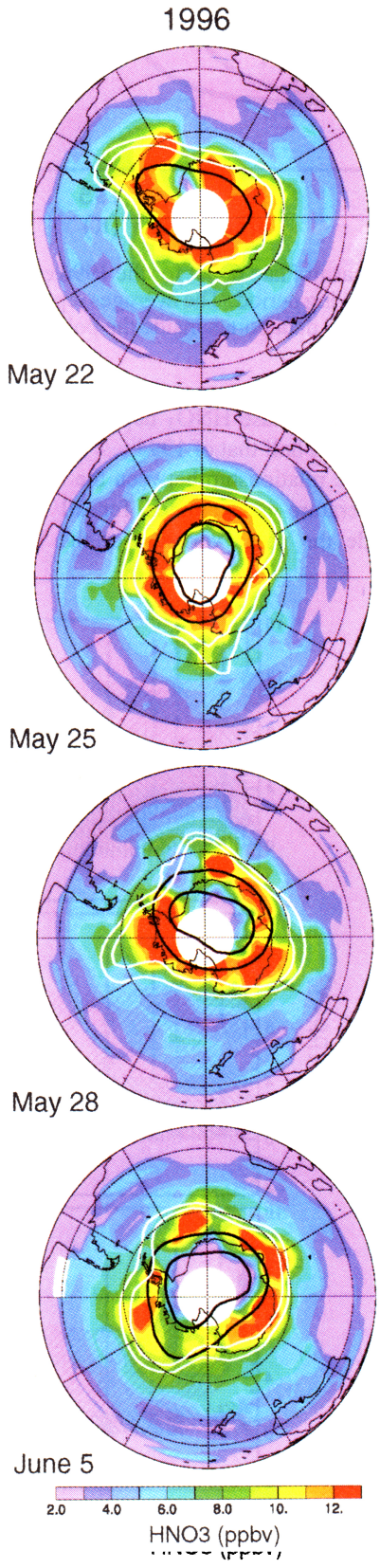

Plate 16. Same as in Plate 1, but for the 1996 early southern winter south viewing period.

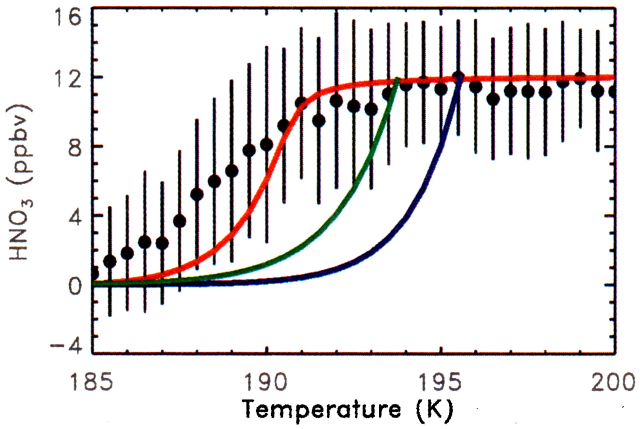

Plate 17. Same as in Plate 6, but for the 1996 early southern winter south viewing period. The averages represent approximately 2800 MLS data points inside the polar vortex.

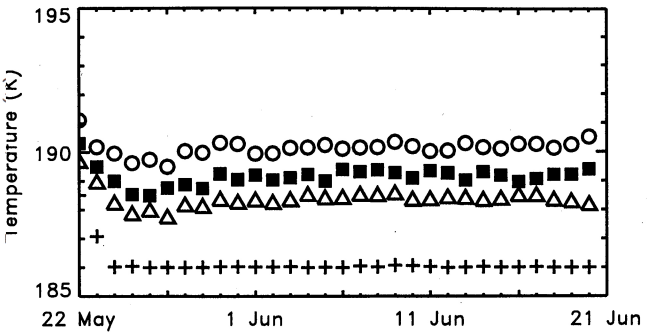

Figure 3. Same as in Figure 2, but for the 1996 early southern winter south viewing period. Again, the minimum temperatures within the vortex as a whole, which are not shown, are much lower.

atures in 1996, gas-phase HNO_3 depletion proceeds at an initial rate less than half that of 1994.

As before, the relationship between the observed HNO_3 and the temperature is examined for all measurements obtained inside the polar vortex over the UARS month (Plate 17). In contrast to the behavior seen in previous years, in 1996 the ternary model does not produce a good match to the MLS data; rather, it overpredicts the degree of HNO_3 depletion at the lowest temperatures. Model calculations are also performed within the annuli enclosed by the 186-K and the 195-, 193-, and 191-K temperature contours. Figure 3 illustrates the uniformly low average temperatures within

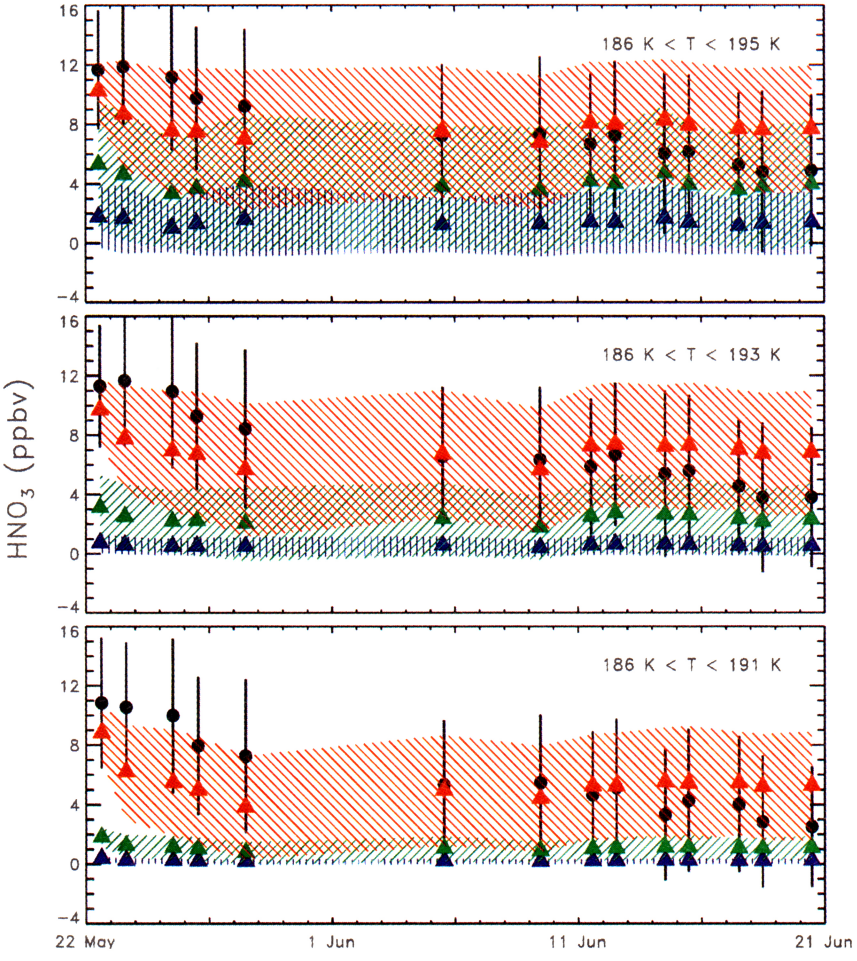

Plate 18a. Same as in Plate 7, but for the 1996 early southern winter south viewing period, using a HNO_3 mixing ratio of 12 ppbv, background aerosol conditions, and a H_2O mixing ratio of 4.5 ppmv.

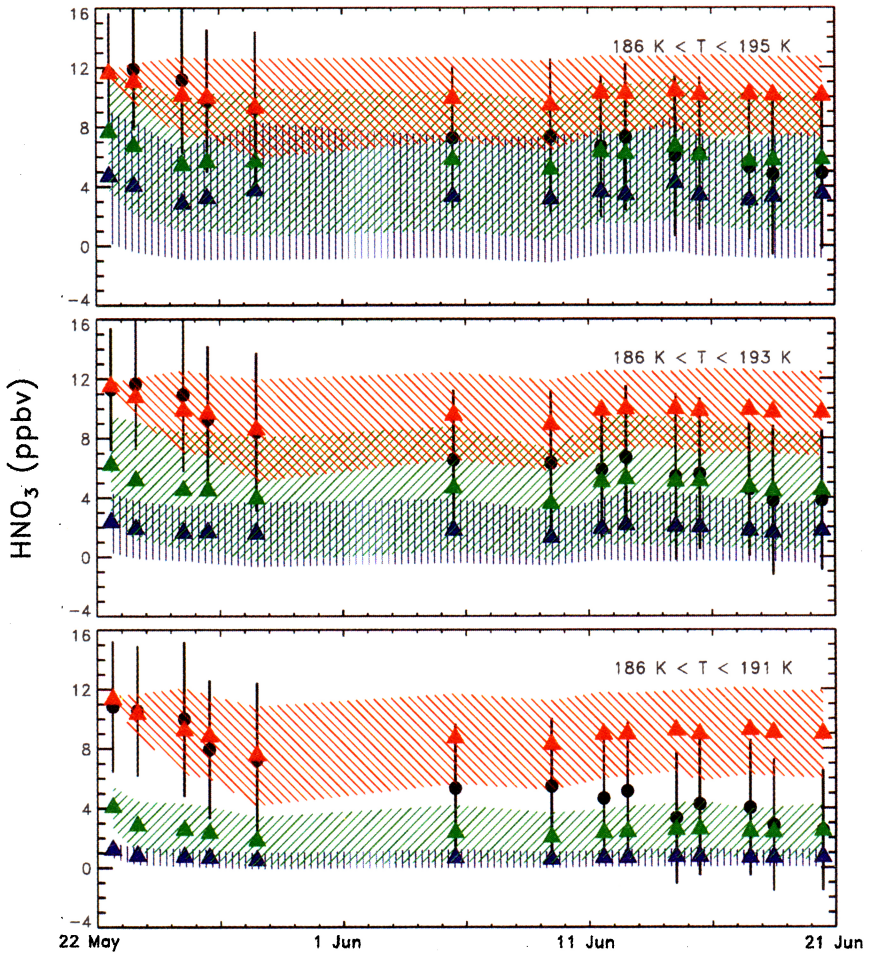

Plate 18b. Same as in Plate 18a, but for a H_2O mixing ratio of 3.0 ppmv.

these regions throughout the observing period. In Plate 18a we show the time series of observed HNO_3 mixing ratios averaged within the low-temperature regions along with those predicted by the various PSC composition models using the standard values of H_2O=4.5 ppmv, HNO_3=12 ppbv, and H_2SO_4=0.3 $\mu g/m^3$. Again, in contrast to the results for earlier years, in 1996 the ternary solution model initially overestimates the degree of HNO_3 uptake. There is some indication in Plate 18a that the agreement with the data improves by the middle of the month for a ternary composition; this may be significant or it may simply be a coincidence since the MLS data exhibit a decreasing trend throughout this period.

It is unlikely that nonequilibrium conditions can explain the 1996 MLS observations. As discussed in section 4.1, even under conditions of rapid cooling liquid ternary solutions maintain a nearly equilibrium composition. A nonequilibrium mixture of NAT or NAD particles and ternary droplets is possible, but in this case the resulting HNO_3 vapor pressure would be between those of the solid and liquid phases. That is, if a majority of the particles are liquid, then gas-phase HNO_3 depletion would be at least as large as that due to HNO_3 uptake into ternary solutions; the presence of some solid particles (over which the HNO_3 vapor pressure is lower) would lead to even greater gas-phase HNO_3 loss. Since the observed HNO_3 vapor pressure in Plate 18a is higher than that predicted by either NAT/NAD or ternary models, a cloud of mixed NAT/NAD and ternary phases can be ruled out.

To explore the possibility that the lack of agreement between the ternary model and the data arises because the assumed abundance of available HNO_3 (12 pbbv) is too low, we have run the ternary model with the total HNO_3 mixing ratio set to 15 ppbv (not shown). While a slightly better fit to the data is achieved for the 195-K contour average, improvements for the averages at lower temperatures are negligible. Results from a second sensitivity test in which the H_2O mixing ratio is reduced to 3 ppmv, while the HNO_3 mixing ratio is kept at 12 ppbv, are shown in Plate 18b. This case yields behavior more akin to that seen in previous years, with an excellent match to the data provided by the ternary model during the initial HNO_3 depletion and by the NAD model thereafter.

Although the HNO_3 and H_2O abundances utilized in Plate 18b allow a good match to the MLS data to be achieved, they may not be representative of actual stratospheric conditions. As discussed in section 4.1, water vapor mixing ratios at the beginning of the winter season would

typically be expected to be in the range of 4–5 ppmv. Values of 3 ppmv or less have been measured inside the vortex in August and September [*Kelly et al.*, 1989; *Santee et al.*, 1995], but these measurements followed the period of extensive dehydration due to the sedimentation of type II (water ice) PSCs. Sufficient time has not elapsed since the onset of low temperatures for significant dehydration to have occurred by May 22, but even if it had, a concomitant diminution of the HNO_3 should have been observed. Type II PSCs also incorporate HNO_3 vapor, either through the simultaneous cocondensation of HNO_3 and H_2O molecules during ice growth or as NAT particles that serve as condensation nuclei for ice crystals [*Toon et al.*, 1989; *Turco et al.*, 1989]. Thus it seems unlikely that the H_2O mixing ratios could have dropped to relatively low levels while the HNO_3 mixing ratios remained undiminished.

Alternatively, it may be that temperatures fell to sufficiently low values sufficiently quickly that a majority of the background sulfate aerosols froze, precluding the formation of ternary solutions. The presence of at least some frozen sulfate cores would promote the growth of a HNO_3/H_2O solid phase referred to as a type Ic PSC by *Tabazadeh and Toon* [1996]. Laboratory studies of the deposition of H_2O and HNO_3 vapors onto a solid surface (either glass or SAT) [*Hanson*, 1992; *Marti and Mauersberger*, 1993; *Iraci et al.*, 1995] have found evidence for the formation of a metastable water-rich HNO_3-containing solid phase over which the HNO_3 vapor pressure is relatively high (as much as 10–20 times higher than that over NAT). As this HNO_3/H_2O solid phase would also be characterized by a higher HNO_3 vapor pressure than a ternary solution, its formation could explain the initial discrepancy between the ternary model and the MLS data in Plate 18a. In this case, the better agreement between the measured HNO_3 and the NAD model at the end of the observing period could indicate the transfer of vapor from the water-rich solid to NAD as the particles age. A new class of large, water-rich particles has been postulated by *Shibata et al.* [1997] to explain ground-based Arctic lidar measurements that do not conform to the existing type Ia/b PSC definitions. Evidence to support the formation of a water-rich HNO_3/H_2O solid phase has also been reported by *Tabazadeh et al.* [1995] and *Tabazadeh and Toon* [1996] from an analysis of aircraft observations of PSCs in both the Arctic and the Antarctic. They found the initial depletion of gas-phase HNO_3 due to a type Ic PSC to be only about 2–3 ppbv, which corresponds very closely to the MLS observations shown in Plate 18.

5. Trajectory Calculations

In the PSC formation scenario of *Tabazadeh et al.* [1994a, 1995, 1996] briefly described above, the thermal history of the air mass is critical to the phase of the PSC since it determines the physical state of the preexisting aerosols. These aerosols are liquid in an air mass that either has never been exposed to temperatures low enough for the H_2SO_4 to freeze as SAT (i.e., near the ice frost point [e.g., *Middlebrook et al.*, 1993; *Koop et al.*, 1995]) or has recently experienced temperatures high enough for SAT to melt (i.e., about 210–220 K [*Middlebrook et al.*, 1993; *Zhang et al.*, 1993b]). On the other hand, the aerosols may freeze through a cooling to temperatures near the ice frost point. In addition, *Iraci et al.* [1994] and *Tabazadeh et al.* [1995] have proposed that after experiencing low temperatures, the H_2SO_4 aerosols may crystallize to SAT upon subsequent warming to about 196–198 K (as observed in the laboratory by *Iraci et al.* [1994]).

To investigate the correlation between synoptic-scale temperature history and PSC composition as inferred from MLS measurements of gas-phase HNO_3, we perform 20-day back trajectory calculations for selected days in each year. As described in more detail by *Manney et al.* [1994], the three-dimensional calculations use horizontal winds and temperatures from the UKMO data assimilation system [*Swinbank and O'Neill*, 1994]. The trajectory code is formulated in isentropic coordinates and employs a standard fourth-order Runge-Kutta scheme. To account for diabatic effects, a recent version of the middle atmosphere radiation code (MIDRAD) first described by *Shine* [1987] is used to compute vertical velocities ($d\theta/dt$). Since MLS data do not provide uninterrupted daily coverage, a climatological ozone field is used for the radiation calculations. The impact on the heating rates of using climatological rather than MLS ozone was determined to be negligible by *Manney et al.* [1994]. Although, in general, the large-scale air motion is simulated well by these calculations, *Manney et al.* [1995b] found that they underestimated the magnitude of the diabatic descent in the 1992 Antarctic early winter, based on comparisons with passive tracers measured by CLAES on UARS.

For each trajectory run, parcels are initialized at 465 K in a box defined within the region inside the vortex where HNO_3 mixing ratios are below 4 ppbv; the total number of parcels in the box is chosen to be 100 (10 on a side), 400 (20 on a side), or 900 (30 on a side), depending on the geographic extent of the HNO_3 depletion on that day. The initialization time is 1200 UT, and parcel positions are saved every 4 hours. Temperature histories are then constructed by interpolating UKMO temperatures (available once daily, at 1200 UT) to the time, latitude, longitude, and θ values of these parcels throughout the 20-day run. Overall diabatic effects are found to be essentially similar for runs in all five years, with parcels descending approximately 20 K in the 20 days leading up to the initialization day.

Temperature histories for selected days during the 1994 PSC formation period are shown in Figure 4. Parcels initialized inside the small area of depleted HNO_3 on June 7 (see Plate 1) had experienced a fairly flat synoptic temperature trend (Figure 4a) prior to cooling below 192 K in the last 24 hours. Trajectories run back from the next 6 days exhibit similar features: The parcels experienced large temperature excursions, but they did not undergo significant or sustained cooling until a precipitous drop in temperature (to the ice frost point or below) occurred during the day before the initialization day. This behavior is illustrated in Figure 4b for June 11. The large temperature oscillations in 1994 arose from a combination of the strength and direction of the winds and the shape and location of the low-temperature

areas relative to the vortex. Since a new set of parcels was brought into the cold region each day, ternary solution PSCs continued to form, but the exposure time to low temperatures was too short for the phase transformation to NAD to occur.

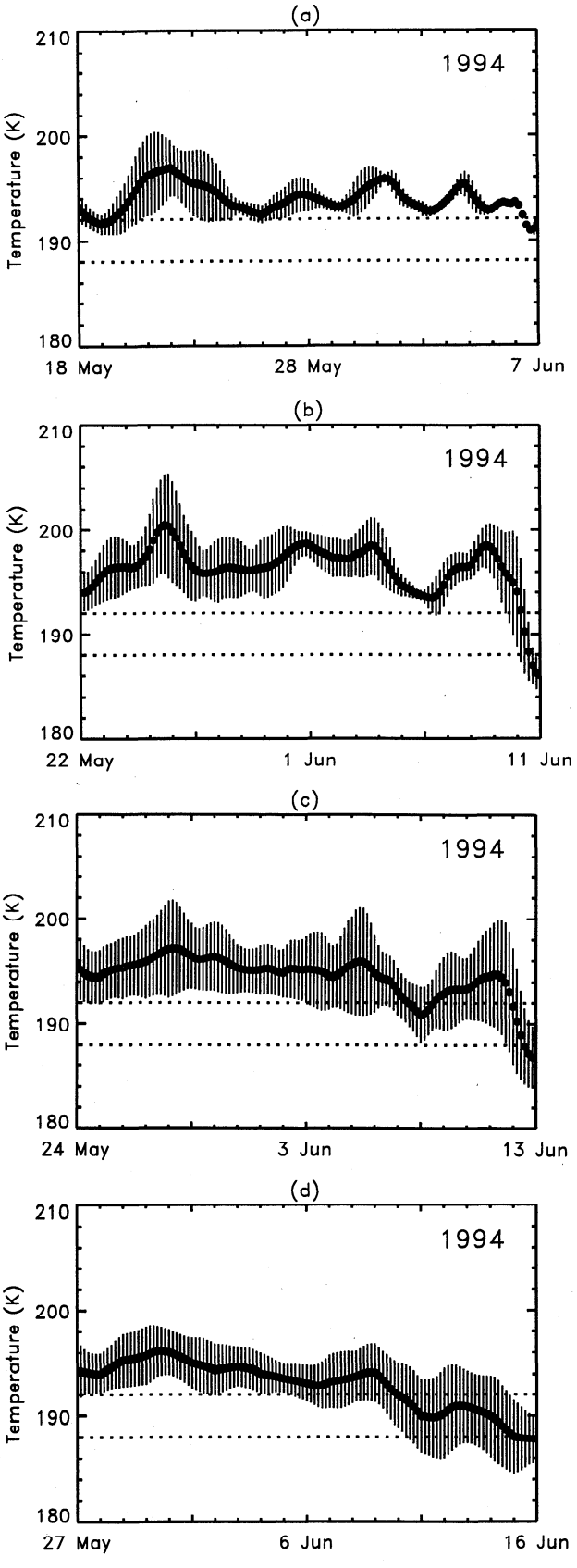

This is consistent with the results shown in Plates 5 and 7, which indicate best agreement with the ternary model at this time. By June 13 (Figure 4c), conditions were such that the average temperature of the parcels had briefly dipped below 192 K about 6 days earlier; this may have triggered the formation of some ternary solution PSCs which then converted to NAD, resulting in a mixed cloud as new ternary solutions formed when the temperatures again fell below 192 K on the day before the initialization day. Not until June 16 (Figure 4d) had the parcels initialized within the low-HNO_3 region experienced low temperatures for an extended period of time. Observed HNO_3 for this and subsequent days is most consistent with the NAD model (Plates 5 and 7), suggesting that exposure to low temperatures for at least several days is necessary for significant formation of NAD.

In Figure 5 we show temperature histories for selected days during the early part of the 1993 observing period. Trajectories from the small area of depleted HNO_3 on May 29 (the first day of the observing period; see Plate 12) indicate that these parcels had cooled below 192 K within the last 24 hours (Figure 5a). This pattern of recent cooling below 192 K for parcels originating within the low-HNO_3 region continued through June 1 (Figure 5b). Although some of the aerosols may have undergone crystallization upon warming from ~192 K to above 196 K, in general, the temperature histories are such that a majority of the preexisting aerosols were probably in a liquid state, setting the stage for the formation of ternary solution PSCs. By June 2 (Figure 5c), the area of depleted HNO_3 was more extensive (see Plate 12), and the average temperature of the parcels initialized in this region had been continuously at or below 192 K for almost 3 days and had hovered around 192 K for several days before that. Similarly, by June 7 (Figure 5d) the parcels initialized in the low-HNO_3 region had, on average, experienced temperatures at or below 192 K for almost 8 days. Despite the prolonged exposure of these parcels to low temperatures, the model calculations of Plate 14 indicate that better agreement with the data is still achieved at this time using a ternary rather than a NAD composition. As in section 4.3, we attribute this delay in the conversion to NAD to the residual enhancement in aerosol loading from the eruption of Mount Pinatubo.

In both 1992 and 1995, MLS data sampling during early southern winter was limited, and PSC formation was already well underway by the time observations of the southern high latitudes resumed. The extent of HNO_3 loss on the first day of the observing period in these years (June 2 and June 7,

Figure 4. Temperature histories along 20–day back trajectories for the ensemble of parcels located within the region inside the vortex where HNO_3 concentrations are less than 4 ppbv on (a) June 7, 1994, (b) June 11, 1994, (c) June 13, 1994, and (d) June 16, 1994. Dashed lines indicate T = 188 K and 192 K. The black circles represent the average temperatures of these parcels at each time step (every 4 hours), and the error bars represent the standard deviations in the averages.

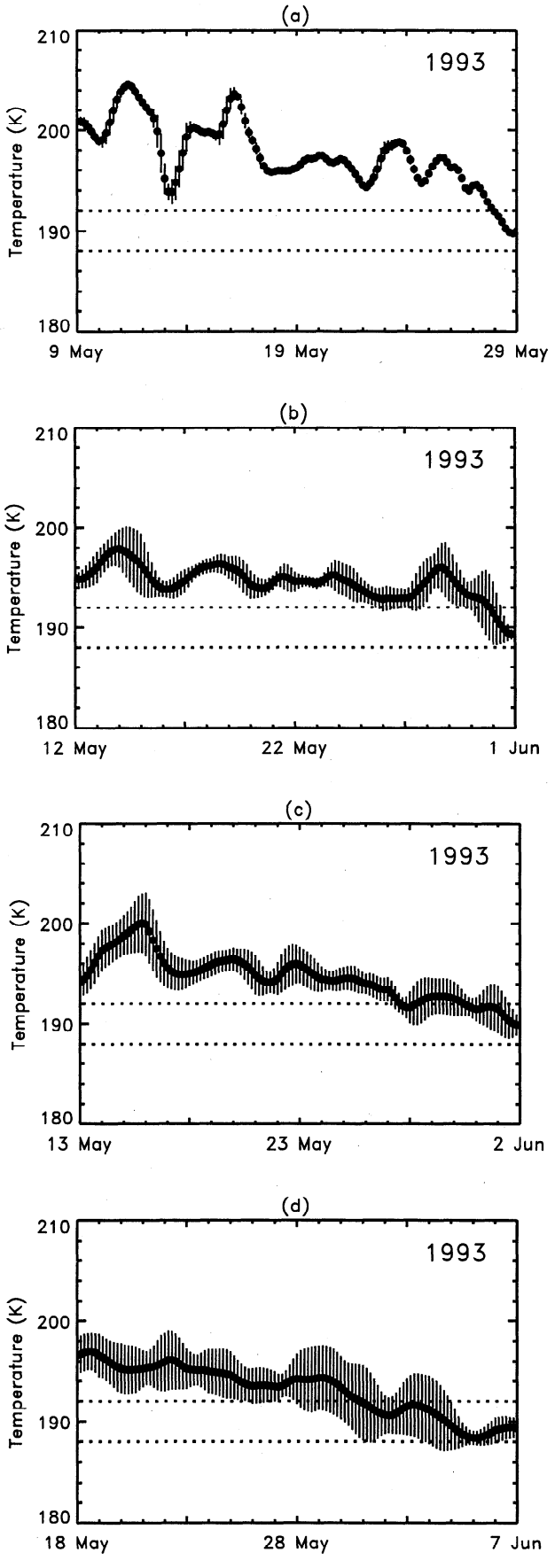

Figure 5. Same as in Figure 4, for (a) May 29, 1993, (b) June 1, 1993, (c) June 2, 1993, and (d) June 7, 1993.

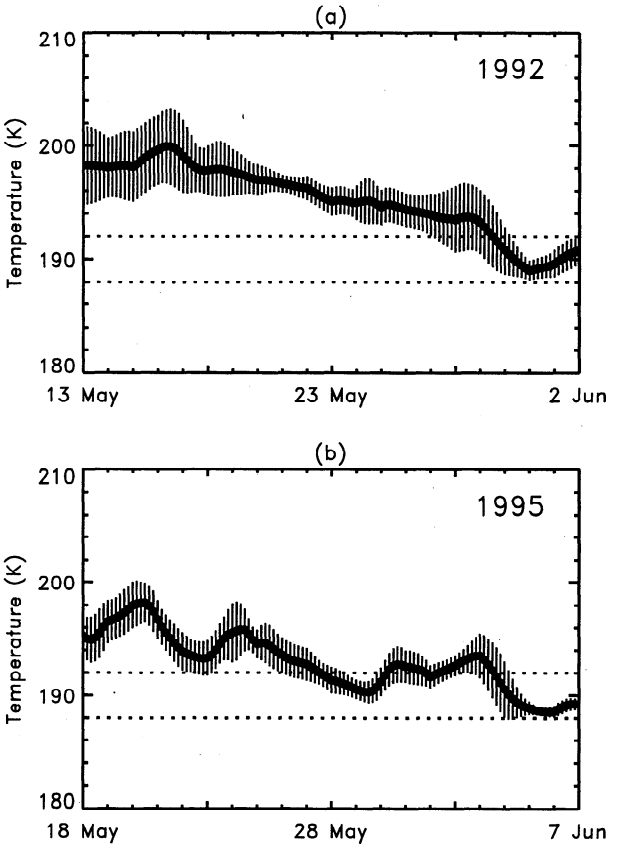

Figure 6. Same as in Figure 4, for (a) June 2, 1992, and (b) June 7, 1995.

respectively) is similar (see Figure 1). In Figure 6a we show the temperature histories of parcels initialized within the low-HNO_3 region on June 2, 1992. In the preceding weeks these parcels experienced a more or less steady temperature decline, and the preexisting aerosols were probably in a liquid state. Just prior to the observation day, the parcels were exposed to temperatures below 192 K for about 3 days, despite a slight warming trend. These conditions are consistent with the formation of ternary solutions. Because 3 days probably would not have allowed sufficient time for NAD nucleation, particularly under the greatly enhanced aerosol loading still present from the Mount Pinatubo eruption (see above), it is likely that the low-HNO_3 observed on June 2 was due to a persistent ternary phase (compare with Plate 10). However, our observations do not exclude a NAD composition. By 1995 the aerosol loading had essentially returned to background levels. The temperature histories of the parcels originating within the low-HNO_3 region on June 7, 1995, are shown in Figure 6b. These parcels had experienced temperatures below 192 K around 8–10 days earlier and had been continuously below 192 K for more than 3 days, allowing time for an initial ternary phase to transform into NAD, as suggested by the observations discussed in section 4.4.

Finally, temperature histories for the 1996 PSC formation period are shown in Figure 7. The average temperature of the parcels initialized inside the small area of depleted HNO_3 on

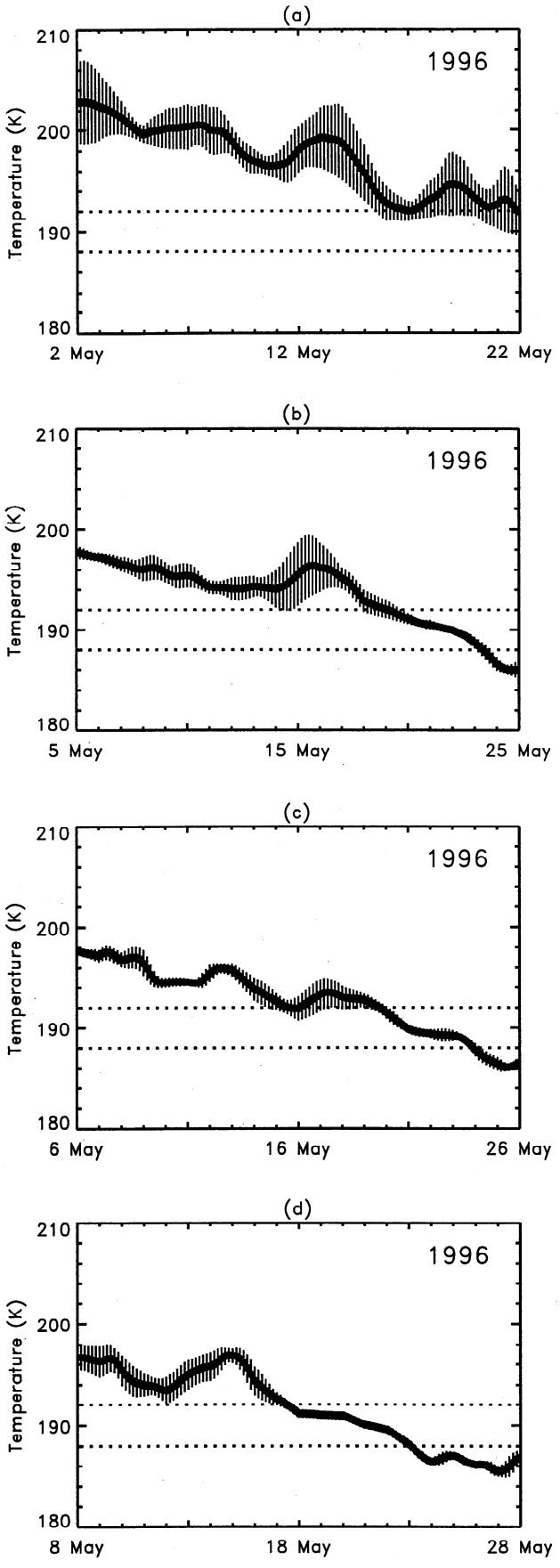

Figure 7. Same as in Figure 4, for (a) May 22, 1996, (b) May 25, 1996, (c) May 26, 1996, and (d) May 28, 1996.

May 22 (see Plate 16) had just dropped to 192 K (Figure 7a); however, the average temperature had been this low on two previous occasions, after which some portion of the parcels encountered temperatures above 196 K. By May 25 and 26 (Figures 7b and 7c), the parcels had been exposed to temperatures below 192 K for more than 6 days and below 188 K for 2 days, and by May 28 (Figure 7d) the parcels had been exposed to temperatures below 192 K for 11 days and below 188 K for 5 days; yet in all these cases the MLS data indicate higher gas-phase HNO_3 values than predicted by any of the PSC composition models (see Plate 18). The parcels originating within the low-HNO_3 region on these days experienced larger sustained synoptic cooling rates and spent more time at temperatures near the ice frost point than in previous years. Hence a larger fraction of the sulfate aerosols may have frozen in the early winter of 1996, inhibiting the growth of ternary solutions. The presence of frozen sulfate cores would lead to the emergence of type Ic PSCs, whose relatively high HNO_3 vapor pressure provides the best match to the pattern of depletion seen in the 1996 MLS HNO_3 data.

6. Summary and Implications

We have examined MLS HNO_3 measurements obtained at the beginning of five southern hemisphere winters: 1992–1996. The observed evolution of the gas-phase HNO_3 was compared against that predicted by NAT [*Hanson and Mauersberger*, 1988], NAD [*Worsnop et al.*, 1993], and liquid ternary solution [*Tabazadeh et al.*, 1994b] models and correlated with temperature histories from three-dimensional back trajectory calculations to infer the composition of the PSCs that formed in early winter each year.

MLS observations of the changes in gas-phase HNO_3 suggest that the first PSCs to form are composed of either liquid ternary solutions or a metastable water-rich solid phase, depending on the physical state of the background sulfate aerosols. This is consistent with the PSC formation scenario of *Tabazadeh et al.* [1994a, 1995, 1996]. According to this scenario, if the preexisting aerosols are liquid, then ternary solutions form as the temperature drops below about 192 K, a few degrees below the NAT condensation point. After prolonged exposure to low temperatures, NAT or NAD particles begin to nucleate, and a mixed cloud results while a transfer of HNO_3 vapor from the ternary solution droplets to the more stable crystalline particles takes place, with eventual complete conversion. This paradigm can explain the MLS 1994 observations, which show better agreement with the ternary solution model in the initial stages of PSC formation but which are matched best by the NAD model as time progresses and the air masses have been exposed to low temperatures for several days. Although the 1995 MLS data are too sparse to allow a definitive conclusion, they also appear to be consistent with this PSC formation scenario.

The basic PSC formation process outlined above also applies to MLS measurements from 1993, when the stratospheric particle optical depth was still elevated by roughly a factor of 10 following the eruption of Mount Pinatubo

[*Russell et al.*, 1996]. However, the 1993 MLS data indicate that HNO_3 uptake into ternary solutions occurs at higher temperatures under enhanced aerosol conditions, as predicted by *Carslaw et al.* [1994] and *Tabazadeh et al.* [1994b]. In addition, the data suggest that the conversion to NAD is delayed under volcanic conditions, since even after the air masses have experienced temperatures below 192 K for almost 8 days the ternary model still provides a better match to the data than the NAD model. This is probably related to the significant differences in composition between ternary solutions formed under volcanic conditions and those formed under background aerosol conditions [*Tabazadeh et al.*, 1994b]. These compositional differences during volcanically perturbed periods may result in changes in the NAD saturation ratio that hinder the formation of crystalline PSCs. After exposure to low temperatures for about 2 weeks, however, the 1993 MLS data are matched best by the NAD model. The MLS data for 1992, when the stratospheric particle optical depth was enhanced by roughly a factor of 20–30 over pre-Pinatubo levels [*Russell et al.*, 1996], may also indicate a persistent ternary phase, but again, the data are too sparse to conclusively distinguish between NAD and ternary solution compositions.

MLS measurements from 1996 indicate less HNO_3 depletion than predicted by any of the PSC composition models. During the 1996 early southern winter the lower stratosphere was substantially colder than average, and the air masses participating in the initial HNO_3 depletion experienced larger sustained synoptic cooling rates and spent more time at temperatures near the ice frost point than in the previous years. Hence a majority of the sulfate aerosols may have frozen in the 1996 early winter, inhibiting the growth of ternary solutions. According to the PSC formation mechanism of *Tabazadeh et al.* [1994a, 1995, 1996], background aerosols in a frozen state promote the initial formation of a metastable water-rich HNO_3-containing solid phase (type Ic), over which the HNO_3 vapor pressure is relatively high. The 1996 MLS HNO_3 data are consistent with the magnitude of the gas-phase HNO_3 depletion attributed to type Ic PSCs by *Tabazadeh and Toon* [1996]. Better agreement between the measured HNO_3 and the NAD model at the end of the observing period may indicate the transfer of vapor from the water-rich solid to NAD as the particles age. Some type Ic PSCs may also have formed in the previous years studied, but their presence would have been masked by the much greater uptake of HNO_3 into ternary solutions if most of the background aerosols were liquid.

In general, we have found a strong correspondence between the area of gas-phase HNO_3 loss and the area of temperatures below 192 K but only a weak correspondence between the area of gas-phase HNO_3 loss and the area of temperatures below 195 K, the value commonly assumed as the threshold for PSC formation. In fact, for the 3 years in which MLS made measurements at or near the time of initial PSC formation (1993, 1994, and 1996), large NAT supersaturations persisted for days to weeks before significant depletion of gas-phase HNO_3 occurred. Although the temperatures were low enough to maintain NAT PSCs, the MLS data indicate that they were not forming, at least not over spatial scales comparable to or larger than the $\sim 400 \times 100 \times 5$ km MLS field of view.

Although our results are strongly suggestive, the limited precision and spatial resolution of the data and the necessity of estimating unmeasured quantities preclude conclusive identification of PSC compositions. With this caveat in mind, however, it appears that the ternary solution and NAD models provide good agreement with the MLS HNO_3 measurements at different stages of the PSC formation process, while the NAT model consistently overestimates the observed removal of gas-phase HNO_3. This has important implications for theoretical studies of ozone depletion. Many stratospheric models employ PSC parameterizations whereby it is assumed that NAT particles form and heterogeneous processing begins immediately after temperatures drop below 195 K. Since most such models have a horizontal resolution similar to that of the MLS data, our results suggest that these models may not calculate ozone loss accurately.

The majority of the MLS HNO_3 measurements obtained during the early southern winter periods indicate that exposure to low temperatures for at least several days (longer under conditions of enhanced aerosol loading following volcanic eruptions) is necessary for a significant degree of crystalline PSC formation. This suggests the existence of substantial free-energy barriers to nucleation for the crystalline forms. That the MLS data agree better with NAD for aged PSCs is supportive of the suggestion of a lower barrier to nucleation for NAD than for NAT [*Worsnop et al.*, 1993; *Disselkamp et al.*, 1996]. In any case, large barriers to nucleation would allow activation and growth of only a small fraction of available condensation nuclei (regardless of cooling rates) and so would result in formation of a small number of relatively large HNO_3-containing particles that could fall appreciable distances, leading to denitrification [*Salawitch et al.*, 1989].

In situ [e.g., *Fahey et al.*, 1990] and satellite [*Roche et al.*, 1994; *Santee et al.*, 1995] observations have shown that both the temporal and the spatial scale of denitrification are substantially greater in the Antarctic than in the Arctic, consistent with the generally warmer and weaker lower stratospheric vortex [e.g., *Andrews*, 1989] and fewer, shorter-duration PSC occurrences [*Poole and Pitts*, 1994] in the northern hemisphere. However, enhanced ClO abundances, arising through reactions on the surfaces of PSC particles, comparable to those over Antarctica are routinely observed throughout the Arctic polar vortex [e.g., *Waters et al.*, 1993; *Santee et al.*, 1995]. Interhemispheric differences in the severity of ozone loss have been ascribed to the moderating influence of high levels of HNO_3 on active chlorine during the latter stages of Arctic winter [e.g., *Brune et al.*, 1991; *Santee et al.*, 1995]. The MLS HNO_3 data presented here suggest that small liquid droplets form quickly at temperatures below $\sim$192 K, initiating chlorine activation, but air masses must be exposed to low temperatures for several days or longer to facilitate growth of the large crystalline particles that undergo significant gravitational settling. Since in

the Arctic the low temperatures are usually confined to relatively small regions that are not concentric with the vortex, individual air masses rarely experience temperatures below 192 K for extended periods of time. Thus the much smaller degree of denitrification in the Arctic is probably related not only to the lack of temperatures below the water ice frost point (~188 K) but also to the lack of temperatures persistently below ~192 K.

Acknowledgments. We thank K. Kelly, D. Fahey, and J. Wilson for providing ER 2 ASHOE data and M. Fromm for providing POAM data prior to publication. We also thank the UKMO (R. Swinbank and A. O'Neill) for meteorological analyses. We are especially grateful to our MLS colleagues for their efforts in producing the version 4 retrievals. Helpful comments on the manuscript from H. Michelsen, M. Danilin, and S. Wofsy are appreciated, and the referees are acknowledged for their insightful and penetrating reviews. The work at the Jet Propulsion Laboratory, California Institute of Technology, was done under contract with the National Aeronautics and Space Administration.

References

Andrews, D. G., Some comparisons between the middle atmosphere dynamics of the southern and northern hemispheres, *Pure Appl. Geophys.*, *130*, 213–232, 1989.

Anthony, S. E., T. B. Onasch, R. T. Tisdale, R. S. Disselkamp, M. A. Tolbert, and J. C. Wilson, Laboratory studies of ternary $H_2SO_4/HNO_3/H_2O$ particles: Implications for polar stratospheric cloud formation, *J. Geophys. Res.*, *102*, 10,777–10,784, 1997.

Arnold, F., H. Schlager, J. Hoffmann, P. Metzinger, and S. Spreng, Evidence for stratospheric nitric acid condensation from balloon and rocket measurements in the Arctic, *Nature*, *342*, 493–497, 1989.

Austin, J., R. R. Garcia, J. M. Russell III, S. Solomon, and A. F. Tuck, On the atmospheric photochemistry of nitric acid, *J. Geophys. Res.*, *91*, 5477–5485, 1986.

Barath, F. T., et al., The Upper Atmosphere Research Satellite Microwave Limb Sounder instrument, *J. Geophys. Res.*, *98*, 10,751–10,762, 1993.

Beyer, K. D., S. W. Seago, H. Y. Chang, and M. J. Molina, Composition and freezing of aqueous H_2SO_4/HNO_3 solutions under polar stratospheric conditions, *Geophys. Res. Lett.*, *21*, 871–874, 1994.

Beyerle, G., B. Luo, R. Neuber, T. Peter, and I. S. McDermid, Temperature dependence of ternary solution particle volumes as observed by lidar in the Arctic stratosphere during winter 1992/1993, *J. Geophys. Res.*, *102*, 3603–3609, 1997.

Borrmann, S., S. Solomon, J. E. Dye, D. Baumgardner, K. K. Kelly, and K. R. Chan, Heterogeneous reactions on stratospheric background aerosols, volcanic sulfuric acid droplets, and type I polar stratospheric clouds: Effects of temperature fluctuations and differences in particle phase, *J. Geophys. Res.*, *102*, 3639–3648, 1997.

Browell, E. V., et al., Large scale variations in ozone and polar stratospheric clouds measured with airborne lidar during formation of the 1987 ozone hole over Antarctica, *NASA Conf. Publ.*, *10014*, 61–64, 1988.

Browell, E. V., C. F. Butler, S. Ismail, P. A. Robinette, A. F. Carter, N. S. Higdon, O. B. Toon, M. R. Schoeberl, and A. F. Tuck, Airborne lidar observations in the wintertime Arctic stratosphere: Polar stratospheric clouds, *Geophys. Res. Lett.*, *17*, 385–388, 1990.

Brune, W. H., J. G. Anderson, D. W. Toohey, D. W. Fahey, S. R. Kawa, R. L. Jones, D. S. McKenna, and L. R. Poole, The potential for ozone depletion in the Arctic polar stratosphere, *Science*, *252*, 1260–1266, 1991.

Butchart, N., and E. E. Remsberg, The area of the stratospheric polar vortex as a diagnostic for tracer transport on an isentropic surface, *J. Atmos. Sci.*, *43*, 1319–1339, 1986.

Carleton, K. L., D. M. Sonnenfroh, W. T. Rawlins, B. E. Wyslouzil, and S. Arnold, Freezing behavior of single sulfuric acid aerosols suspended in a quadrupole trap, *J. Geophys. Res.*, *102*, 6025–6033, 1997.

Carslaw, K. S., B. P. Luo, S. L. Clegg, T. Peter, P. Brimblecombe, and P. J. Crutzen, Stratospheric aerosol growth and HNO_3 gas phase depletion from coupled HNO_3 and water uptake by liquid particles, *Geophys. Res. Lett.*, *21*, 2479–2482, 1994.

Clapp, M. L., R. F. Niedziela, L. J. Richwine, T. Dransfield, R. E. Miller, and D. R. Worsnop, Infrared spectroscopy of sulfuric acid/water aerosols: Freezing characteristics, *J. Geophys. Res.*, *102*, 8899–8907, 1997.

Climate Prediction Center, National Center for Environmental Prediction, Southern hemisphere winter summary, 1996, Nat. Oceanic and Atmos. Admin., Washington, D. C., 1996.

Crutzen, P. J., and F. Arnold, Nitric acid cloud formation in the cold Antarctic stratosphere: A major cause for the springtime "ozone hole", *Nature*, *324*, 651–655, 1986.

de Zafra, R. L., V. Chan, S. Crewell, C. Trimble, and J. M. Reeves, Millimeter wave spectroscopic measurements over the south pole, 3, The behavior of stratospheric nitric acid through polar fall, winter, and spring, *J. Geophys. Res.*, *102*, 1399–1410, 1997.

Del Negro, L. A., et al., Evaluating the role of NAT, NAD, and liquid $H_2SO_4/H_2O/HNO_3$ solutions in Antarctic polar stratospheric cloud aerosol: Observations and implications, *J. Geophys. Res.*, *102*, 13,255–13,282, 1997.

Disselkamp, R. S., S. E. Anthony, A. J. Prenni, T. B. Onasch, and M. A. Tolbert, Crystallization kinetics of nitric acid dihydrate aerosols, *J. Phys. Chem.*, *100*, 9127–9137, 1996.

Drdla, K., A. Tabazadeh, R. P. Turco, M. Z. Jacobson, J. E. Dye, C. Twohy, and D. Baumgardner, Analysis of the physical state of one Arctic polar stratospheric cloud based on observations, *Geophys. Res. Lett.*, *21*, 2475–2478, 1994.

Dye, J. E., B. W. Gandrud, D. Baumgardner, K. R. Chan, G. V. Ferry, M. Loewenstein, K. K. Kelly, and J. C. Wilson, Observed particle evolution in the polar stratospheric cloud of January 24, 1989, *Geophys. Res. Lett.*, *17*, 413–416, 1990.

Dye, J. E., D. Baumgardner, B. W. Gandrud, S. R. Kawa, K. K. Kelly, M. Loewenstein, G. V. Ferry, K. R. Chan, and B. L. Gary, Particle size distributions in Arctic polar stratospheric clouds, growth and freezing of sulfuric acid droplets, and implications for cloud formation, *J. Geophys. Res.*, *97*, 8015–8034, 1992.

Dye, J. E., et al., In situ observations of an Antarctic polar stratospheric cloud: Similarities with Arctic observations, *Geophys. Res. Lett.*, *23*, 1913–1916, 1996.

Fahey, D. W., K. K. Kelly, G. V. Ferry, L. R. Poole, J. C. Wilson, D. M. Murphy, M. Loewenstein, and K. R. Chan, In situ measurements of total reactive nitrogen, total water, and aerosol in a polar stratospheric cloud in the Antarctic, *J. Geophys. Res.*, *94*, 11,299–11,315, 1989.

Fahey, D. W., K. K. Kelly, S. R. Kawa, A. F. Tuck, M. Loewenstein, K. R. Chan, and L. E. Heidt, Observations of denitrification and dehydration in the winter polar stratospheres, *Nature*, *344*, 321–324, 1990.

Fox, L. E., D. R. Worsnop, M. S. Zahniser, and S. C. Wofsy, Metastable phases in polar stratospheric aerosols, *Science*, *267*, 351–355, 1995.

Fromm, M. D., J. D. Lumpe, R. M. Bevilacqua, E. P. Shettle, J. Hornstein, S. T. Massie, and K. H. Fricke, Observations of Antarctic polar stratospheric clouds by POAM II: 1994–1996, *J. Geophys. Res.*, *102*, 23,659–23,672, 1997.

Godin, S., G. Mégie, C. David, D. Haner, C. Flesia, and Y. Emery, Airborne lidar observation of mountain-wave-induced

polar stratospheric clouds during EASOE, *Geophys. Res. Lett.*, *21*, 1335–1338, 1994.

Hanson, D., The uptake of HNO_3 onto ice, NAT, and frozen sulfuric acid, *Geophys. Res. Lett.*, *19*, 2063–2066, 1992.

Hanson, D., and K. Mauersberger, Laboratory studies of the nitric acid trihydrate: Implications for the south polar stratosphere, *Geophys. Res. Lett.*, *15*, 855–858, 1988.

Hofmann, D. J., and T. Deshler, Stratospheric cloud observations during formation of the Antarctic ozone hole in 1989, *J. Geophys. Res.*, *96*, 2897–2912, 1991.

Hübler, G., D. W. Fahey, K. K. Kelly, D. D. Montzka, M. A. Carroll, A. F. Tuck, L. E. Heidt, W. H. Pollock, G. L. Gregory, and J. F. Vedder, Redistribution of reactive odd nitrogen in the lower Arctic stratosphere, *Geophys. Res. Lett.*, *17*, 453–456, 1990.

Imre, D. G., J. Xu, and A. C. Tridico, Phase transformations in sulfuric acid aerosols: Implications for stratospheric ozone depletion, *Geophys. Res. Lett.*, *24*, 69–72, 1997.

Iraci, L. T., A. M. Middlebrook, M. A. Wilson, and M. A. Tolbert, Growth of nitric acid hydrates on thin sulfuric acid films, *Geophys. Res. Lett.*, *21*, 867–870, 1994.

Iraci, L. T., A. M. Middlebrook, and M. A. Tolbert, Laboratory studies of the formation of polar stratospheric clouds: Nitric acid condensation on thin sulfuric acid films, *J. Geophys. Res.*, *100*, 20,969–20,977, 1995.

Kawa, S. R., D. W. Fahey, K. K. Kelly, J. E. Dye, D. Baumgardner, B. W. Gandrud, M. Loewenstein, G. V. Ferry, and K. R. Chan, The Arctic polar stratospheric cloud aerosol: Aircraft measurements of reactive nitrogen, total water, and particles, *J. Geophys. Res.*, *97*, 7925–7938, 1992.

Kelly, K. K., et al., Dehydration in the lower Antarctic stratosphere during late winter and early spring, 1987, *J. Geophys. Res.*, *94*, 11,317–11,357, 1989.

Kent, G. S., L. R. Poole, and M. P. McCormick, Characteristics of Arctic polar stratospheric clouds as measured by airborne lidar, *J. Atmos. Sci.*, *43*, 2149–2161, 1986.

Koop, T., U. M. Biermann, W. Raber, B. P. Luo, P. J. Crutzen, and T. Peter, Do stratospheric aerosol droplets freeze above the ice frost point?, *Geophys. Res. Lett.*, *22*, 917–920, 1995.

Kumer, J. B., et al., Comparison of correlative data with HNO_3 version 7 from the CLAES instrument deployed on the NASA Upper Atmosphere Research Satellite, *J. Geophys. Res.*, *101*, 9621–9656, 1996.

Larsen, N., B. M. Knudsen, J. M. Rosen, N. T. Kjome, and E. Kyrö, Balloonborne backscatter observations of type 1 PSC formation: Inference about physical state from trajectory analysis, *Geophys. Res. Lett.*, *23*, 1091–1094, 1996.

Larsen, N., B. M. Knudsen, J. M. Rosen, N. T. Kjome, R. Neuber, and E. Kyrö, Temperature histories in liquid and solid polar stratospheric cloud formation, *J. Geophys. Res.*, *102*, 23,505–23,517, 1997.

Manney, G. L., R. W. Zurek, A. O'Neill, and R. Swinbank, On the motion of air through the stratospheric polar vortex, *J. Atmos. Sci.*, *51*, 2973–2994, 1994.

Manney, G. L., R. W. Zurek, L. Froidevaux, and J. W. Waters, Evidence for Arctic ozone depletion in late February and early March 1994, *Geophys. Res. Lett.*, *22*, 2941–2944, 1995a.

Manney, G. L., et al., Lagrangian transport calculations using UARS data, I, Passive tracers, *J. Atmos. Sci.*, *52*, 3049–3068, 1995b.

Manney, G. L., R. Swinbank, S. T. Massie, M. E. Gelman, A. J. Miller, R. Nagatani, A. O'Neill, and R. W. Zurek, Comparison of U.K. Meteorological Office and U.S. National Meteorological Center stratospheric analyses during northern and southern winter, *J. Geophys. Res.*, *101*, 10,311–10,334, 1996.

Marti, J., and K. Mauersberger, Laboratory simulations of PSC particle formation, *Geophys. Res. Lett.*, *20*, 359–362, 1993.

McCormick, M. P., H. M. Steele, P. Hamill, W. P. Chu, and T. J. Swissler, Polar stratospheric cloud sightings by SAM II, *J. Atmos. Sci.*, *39*, 1387–1397, 1982.

McCormick, M. P., P. Hamill, and U. O. Farrukh, Characteristics of polar stratospheric clouds as observed by SAM II, SAGE, and lidar, *J. Meteorol. Soc. Jpn.*, *63*, 267–276, 1985.

McCormick, M. P., C. R. Trepte, and M. C. Pitts, Persistence of polar stratospheric clouds in the southern polar region, *J. Geophys. Res.*, *94*, 11,241–11,251, 1989.

McCormick, M. P., G. S. Kent, W. H. Hunt, M. T. Osborn, L. R. Poole, and M. C. Pitts, Arctic polar stratospheric cloud observations by airborne lidar, *Geophys. Res. Lett.*, *17*, 381–383, 1990.

Meilinger, S. K., T. Koop, B. P. Luo, T. Huthwelker, K. S. Carslaw, U. Krieger, P. J. Crutzen, and T. Peter, Size-dependent stratospheric droplet composition in lee wave temperature fluctuations and their potential role in PSC freezing, *Geophys. Res. Lett.*, *22*, 3031–3034, 1995.

Mergenthaler, J. L., J. B. Kumer, and A. E. Roche, CLAES south-looking aerosol observations for 1992, *Geophys. Res. Lett.*, *20*, 1295–1298, 1993.

Mergenthaler, J. L., J. B. Kumer, A. E. Roche, and S. T. Massie, Distribution of Antarctic polar stratospheric clouds as seen by the CLAES experiment, *J. Geophys. Res.*, *102*, 19,161–19,170, 1997.

Middlebrook, A. M., L. T. Iraci, L. S. McNeill, B. G. Koehler, M. A. Wilson, O. W. Saastad, and M. A. Tolbert, Fourier transform-infrared studies of thin H_2SO_4/H_2O films: Formation, water uptake, and solid-liquid phase changes, *J. Geophys. Res.*, *98*, 20,473–20,481, 1993.

Molina, M. J., R. Zhang, P. J. Wooldridge, J. R. McMahon, J. E. Kim, H. Y. Chang, and K. D. Beyer, Physical chemistry of the $H_2SO_4/HNO_3/H_2O$ system: Implications for polar stratospheric clouds, *Science*, *216*, 1418–1423, 1993.

Murphy, D. M., and B. L. Gary, Mesoscale temperature fluctuations and polar stratospheric clouds, *J. Atmos. Sci.*, *52*, 1753–1760, 1995.

Poole, L. R., and M. C. Pitts, Polar stratospheric cloud climatology based on Stratospheric Aerosol Measurement II observations from 1978 to 1989, *J. Geophys. Res.*, *99*, 13,083–13,089, 1994.

Pueschel, R. F., et al., Condensed nitrate, sulfate, and chloride in Antarctic stratospheric aerosols, *J. Geophys. Res.*, *94*, 11,271–11,284, 1989.

Ravishankara, A. R., and D. R. Hanson, Differences in the reactivity of type I polar stratospheric clouds depending on their phase, *J. Geophys. Res.*, *101*, 3885–3890, 1996.

Roche, A. E., J. B. Kumer, J. L. Mergenthaler, G. A. Ely, W. G. Uplinger, J. F. Potter, T. C. James, and L. W. Sterritt, The Cryogenic Limb Array Etalon Spectrometer (CLAES) on UARS: Experiment description and performance, *J. Geophys. Res.*, *98*, 10,763–10,775, 1993.

Roche, A. E., J. B. Kumer, J. L. Mergenthaler, R. W. Nightingale, W. G. Uplinger, G. A. Ely, J. F. Potter, D. J. Wuebbles, P. S. Connell, and D. E. Kinnison, Observations of lower-stratospheric $ClONO_2$, HNO_3, and aerosol by the UARS CLAES experiment between January 1992 and April 1993, *J. Atmos. Sci.*, *51*, 2877–2902, 1994.

Russell, P. B., et al., Global to microscale evolution of the Pinatubo volcanic aerosol derived from diverse measurements and analyses, *J. Geophys. Res.*, *101*, 18,745–18,763, 1996.

Salawitch, R. J., G. P. Gobbi, S. C. Wofsy, and M. B. McElroy, Denitrification in the Antarctic stratosphere, *Nature*, *339*, 525–527, 1989.

Santee, M. L., W. G. Read, J. W. Waters, L. Froidevaux, G. L. Manney, D. A. Flower, R. F. Jarnot, R. S. Harwood, and G. E. Peckham, Interhemispheric differences in polar stratospheric HNO_3, H_2O, ClO, and O_3, *Science*, *267*, 849–852, 1995.

Santee, M. L., G. L. Manney, W. G. Read, L. Froidevaux, and J. W. Waters, Polar vortex conditions during the 1995–1996 Arctic winter: MLS ClO and HNO_3, *Geophys. Res. Lett.*, *23*, 3207–3210, 1996.

Santee, M. L., G. L. Manney, L. Froidevaux, R. W. Zurek, and J. W.

Waters, MLS observations of ClO and HNO_3 in the 1996–1997 Arctic polar vortex, *Geophys. Res. Lett.*, *24*, 2713–2716, 1997.

Shibata, T., et al., Polar stratospheric clouds observed by lidar over Spitsbergen in the winter of 1994/1995: Liquid particles and vertical "sandwich" structure, *J. Geophys. Res.*, *102*, 10,829–10,840, 1997.

Shine, K. P., The middle atmosphere in the absence of dynamic heat fluxes, *Q. J. R. Meteorol. Soc.*, *113*, 603–633, 1987.

Solomon, S., Progress towards a quantitative understanding of Antarctic ozone depletion, *Nature*, *347*, 347–354, 1990.

Swinbank, R., and A. O'Neill, A stratosphere-troposphere data assimilation system, *Mon. Weather Rev.*, *122*, 686–702, 1994.

Tabazadeh, A., and O. B. Toon, The presence of metastable HNO_3/H_2O solid phases in the stratosphere inferred from ER 2 data, *J. Geophys. Res.*, *101*, 9071–9078, 1996.

Tabazadeh, A., R. P. Turco, K. Drdla, M. Z. Jacobsen, and O. B. Toon, A study of type I polar stratospheric cloud formation, *Geophys. Res. Lett.*, *21*, 1619–1622, 1994a.

Tabazadeh, A., R. P. Turco, and M. Z. Jacobsen, A model for studying the composition and chemical effects of stratospheric aerosols, *J. Geophys. Res.*, *99*, 12,897–12,914, 1994b.

Tabazadeh, A., O. B. Toon, and P. Hamill, Freezing behavior of stratospheric sulfate aerosols inferred from trajectory studies, *Geophys. Res. Lett.*, *22*, 1725–1728, 1995.

Tabazadeh, A., O. B. Toon, B. L. Gary, J. T. Bacmeister, and M. R. Schoeberl, Observational constraints on the formation of type Ia polar stratospheric clouds, *Geophys. Res. Lett.*, *23*, 2109–2112, 1996.

Tolbert, M. A., Sulfate aerosols and polar stratospheric cloud formation, *Science*, *264*, 527–528, 1994.

Toon, O. B., and M. A. Tolbert, Spectroscopic evidence against nitric acid trihydrate in polar stratospheric clouds, *Nature*, *375*, 218–221, 1995.

Toon, O. B., P. Hamill, R. P. Turco, and J. Pinto, Condensation of HNO_3 and HCl in the winter polar stratospheres, *Geophys. Res. Lett.*, *13*, 1284–1287, 1986.

Toon, O. B., R. P. Turco, J. Jordan, J. Goodman, and G. Ferry, Physical processes in polar stratospheric ice clouds, *J. Geophys. Res.*, *94*, 11,359–11,380, 1989.

Toon, O. B., E. V. Browell, S. Kinne, and J. Jordan, An analysis of lidar observations of polar stratospheric clouds, *Geophys. Res. Lett.*, *17*, 393–396, 1990a.

Toon, O. B., R. P. Turco, and P. Hamill, Denitrification mechanisms in the polar stratospheres, *Geophys. Res. Lett.*, *17*, 445–448, 1990b.

Tuck, A. F., K. K. Kelly, C. R. Webster, M. Loewenstein, R. M. Stimpfle, M. H. Proffitt, and R. K. Chan, Airborne chemistry and dynamics at the edge of the 1994 Antarctic vortex, *J. Chem. Soc., Faraday Trans.*, *91*, 3063–3071, 1995.

Turco, R. P., O. B. Toon, and P. Hamill, Heterogeneous physicochemistry of the polar ozone hole, *J. Geophys. Res.*, *94*, 16,493–16,510, 1989.

Waters, J. W., Microwave limb sounding, in *Atmospheric Remote Sensing by Microwave Radiometry*, edited by M. A. Janssen, pp. 383–496, John Wiley, New York, 1993.

Waters, J. W., L. Froidevaux, W. G. Read, G. L. Manney, L. S. Elson, D. A. Flower, R. F. Jarnot, and R. S. Harwood, Stratospheric ClO and ozone from the Microwave Limb Sounder on the Upper Atmosphere Research Satellite, *Nature*, *362*, 597–602, 1993.

Worsnop, D. R., L. E. Fox, M. S. Zahniser, and S. C. Wofsy, Vapor pressures of solid hydrates of nitric acid: Implications for polar stratospheric clouds, *Science*, *259*, 71–74, 1993.

Zhang, R., P. J. Wooldridge, and M. J. Molina, Vapor pressure measurements for the $H_2SO_4/HNO_3/H_2O$ and $H_2SO_4/HCl/H_2O$ systems: Incorporation of stratospheric acids into background sulfate aerosols, *J. Phys. Chem.*, *97*, 8541–8548, 1993a.

Zhang, R., P. J. Wooldridge, J. P. Abbatt, and M. J. Molina, Physical chemistry of the H_2SO_4/H_2O binary system at low temperatures: Stratospheric implications, *J. Phys. Chem.*, *97*, 7351–7360, 1993b.

L. Froidevaux, G. L. Manney, W. G. Read, R. J. Salawitch, M. L. Santee (corresponding author), and J. W. Waters, Jet Propulsion Laboratory, Mail Stop 183–701, 4800 Oak Grove Drive, Pasadena, CA 91109. (e-mail: mls@mls.jpl.nasa.gov)

A. Tabazadeh, NASA Ames Research Center, Moffett Field, CA 94035. (e-mail: taba@sky.arc.nasa.gov)

(Received April 30, 1997; revised January 27, 1998; accepted January 28, 1998.)